High-entropy materials: critical review and way forward

Nilesh P. Gurao* and Krishanu Biswas*

Department of Materials Science and Engineering, Indian Institute of Technology Kanpur, Kanpur 208 016, India

High-entropy materials and related complex concentrated materials are considered to be the new 'avatar' in physical metallurgy and materials engineering, inspiring novel ideas and approaches to design materials by expanding the compositional space in multicomponent and multiprincipal systems. This article is intended to provide critical analyses of the field, summarizing the principles underlying the birth and growth of these novel materials, progress over the last 15 years, and expansion of the field from metallic alloys to ceramics. Finally, the challenges ahead and possible way forward are discussed.

Keywords: Ceramics, compositional space, high-entropy materials, metallic alloys.

ALLOYING is the greatest gift for the development of human civilization on our planet. We have been using alloying (by the addition of alloying elements to base metals) even since the serendipitous discovery of Cu–Sn bronzes to modify properties for betterment of performance of any material[1]. For example, steels contain iron as the primary element into which carbon, silicon and chromium are added in minute amounts to obtain high strength, corrosion resistance, ductility; copper is added to aluminium to obtain strong and tough duralumin for aircraft; copper–beryllium alloys are made for non-sparking applications in explosive environment, etc. However, the traditional alloys we use are primarily based on one or two elements into which alloying additions are made. In the last decade of the 20th century, it was acknowledged that this primary element-based approach severely restricts the choice of elements and their addition, and hence the field of high-entropy materials (HEMs) started in 2004 in order to 'expand the compositional space' of the multicomponent system[2,3]. This field, including high-entropy alloys (HEAs) and high-entropy ceramics (HECs)[4,5] has gathered momentum as well as scientific and technological curiosity, due to the desire to address fundamental issues achieving extraordinary physical, structural and functional properties for engineering applications from the explored compositional space in different materials[6,7]. The approach is based on mixing multiprincipal elements in relatively high concentration, which is distinctly different from the traditional alloying design approach. Hence, it has opened up new possibilities by providing access to hitherto unexplored compositional and thereby virgin property space. The fundamentals of our understanding of physical metallurgy, thermodynamic, kinetics and properties have been thrown up with challenges that they have prevailed, but our understanding of these aspects has improved with the advent of HEAs[8]. It is no surprise that the new field of HEAs has gradually expanded to include complex concentrated alloys (CCAs)[9,10], which comprise of astronomically large number of combinations. The initial focus from metallic alloys has gradually shifted to ceramics, and other complex concentrated materials (CCMs), leading to evolution of the field. The biggest contribution of HEAs has been towards 'exploring the unexplored compositional space' by thermodynamic modelling, high throughput experiments and combinational alloy development. All the tools and techniques developed for the study of HEAs are expected to yield novel results, and lead serendipitous and tedious alloy development from an art form to a thorough scientific domain. It is, therefore important to look backward in order to chart our way forward in the field of HEAs. There have been many seminal reviews on the topic discussing various aspects related but not limited to fundamental scientific issues, processing, properties and applications of these materials in engineering applications. The focus of this article is to portray our journey in this highly exciting field, which we hope shall encourage young researchers in India and elsewhere to take a plunge into research on HEMs.

Basic concepts

The concept of HEAs and multiprincipal component alloys was proposed independently in 2004 by Yeh and co-workers[11,12] and Cantor *et al.*[13]. However, the concept of exploring central regions of multicomponent phase diagrams has been attempted since the 1960s, particularly with respect to bulk metallic glasses. The major driving force for research was to explore the unexplored regions of the multicomponent phase diagrams, and entropy was not mentioned by Cantor. However, Yeh's approach was to maximize configurational entropy to avoid intermetallic phases which are generally found in the central region

*For correspondence. (e-mail: npgurao@iitk.ac.in; kbiswas@iitk.ac.in)

of any phase diagram and instead focus on stabilized solid solution phases. This led to the nomenclature of multiprincipal multicomponent alloys as HEAs. Based on these concepts, distinct definition of these alloys has been established for the latter case.

Definition of high-entropy materials

Although the strict definition of these alloys is also based on composition and absolute value of configurational entropy, HEAs can be defined in two broad ways[1,6,11]. The composition-based definition describes HEAs as alloys with five or more elements with equal or near-equal proportions (5–35 atomic percentage) of each element. On the other hand, the entropy-based definition of HEAs describes them as alloys with configurational entropy of (ΔS_{mix}) 1.61R, where R is the universal gas constant. This definition categorizes solid solutions as low- (<0.69R), medium- (from 0.69R–1.61R) and high-entropy (>1.61R) alloys, and can be used to classify most metallic alloys. The entropy-based definition of HEAs works well for equiatomic alloys as well. However, there are some exceptions with non-equiatomic HEAs that satisfy the composition-based definition, but have ΔS_{mix} lower than 1.5R (ref. 14). For instance, a quinary alloy $A_{35}B_{35}C_{20}D_5E_5$ will have a ΔS_{mix} of 1.39R that is the same as an equiatomic quaternary alloy and is closer to ΔS_{mix} of superalloy with 12 elements (ΔS_{mix} ~1.37R). In order to avoid confusion, a working definition of >1.5R has been accepted in the literature. At the risk of putting the cart in front of the horse, we would like to state that the recent literature has shown that ternary and even a few binary alloys falling in the medium-entropy criterion also show exciting features similar to HEAs and are now included in the family of CCAs. A similar observation is also made for HECs and all of them constitute the broad family of HEMs. In fact, ΔS_{mix} of multicomponent ceramics is much lower because anions (O, B, C, N) occupy fixed positions and hence, do not have any effect on ΔS_{mix}. It is the cationic arrangement which provides an increase in ΔS_{mix}. Despite the limitation of the entropy-based approach, there is unanimity in the field to consider the concentrated solid solutions of metals and ceramics as HEAs. It is now agreed that alloy systems of metals and metalloids or ceramics with compositions away from the corner and edges of the phase diagram as depicted in Figure 1, can be considered as HEMs.

Four core effects

The four core effects proposed by Yeh and co-workers comprise the high-entropy effect, sluggish diffusion effect, lattice distortion effect and cocktail effect[15,16]. The first three effects are actually hypotheses that were proposed in the early days of high-entropy metal research by Yeh and co-workers, while the cocktail effect was proposed by Ranganathan. These hypotheses have been central to the field of HEAs, and a historical evolution of our understanding of these hypotheses or their reinterpretation with time is presented here.

The high-entropy effect: The high entropy of solid solution phases is central to the field of HEAs, indicating that the higher configurational entropy in equiatomic alloys with five or more elements leads to stabilization of random solid solutions rather than intermetallics. A strict definition based on either composition or absolute value of ΔS_{mix} can cause confusion and we have to keep in mind that both the entropy-based and composition-based definitions are operational in nature, with the former definition being more popular in the literature. Though the original formulation focused only on configurational entropy, in recent years vibrational, electronic and magnetic terms have also been acknowledged[17]. However, it is to be remembered that phase stability is determined by minimization of Gibbs free energy and maximization of entropy only aids in reducing the former. Hence, a holistic view is required for the stability of phases, and enthalpy of mixing is also to be considered in addition to configurational entropy. A negative enthalpy of mixing indicates compound formation or ordering, while a positive enthalpy of mixing indicates phase separation. Thus, in order to obtain a random solid solution stabilized by high configurational entropy, the enthalpy of mixing should not be highly positive. This observation has led to the development of many selection criteria for HEAs. Thus, the high entropy effect is also more correctly referred to as the thermodynamic factor in the subsequent literature as it facilitates random solid solution formation by minimizing Gibbs free energy.

Sluggish diffusion effect: HEAs are random and/or ordered solid solutions, characterized by whole solute matrix with no solvent element to dominate the composition of solid solution phases. This results in difference in the diffusion of an atom in a whole-solute matrix and that

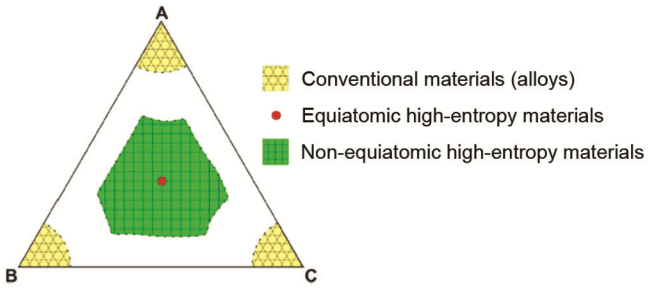

Figure 1. Schematic diagram showing compositional space for high-entropy materials (MEMs). A, B and C are pure elements for high-entropy alloys (HEAs); and they can be oxides, borides or carbides for high-entropy ceramics (HECs; from ref. 14).

of conventional alloys matrix. In HEAs, the neighbouring atom of each lattice site is surrounded by different atoms and hence, the neighbours remain different both before and after an atom occupies a vacancy during diffusion. This difference in local atomic configuration results in different bonding, creating different local energies for each site. It was proposed that such a scenario would lead to sluggish diffusion, i.e. lower diffusion rate in HEAs compared to conventional alloys. Tsai *et al.*[18] attributed large fluctuation in lattice potential energy (LPE) between lattice sites during the movement of an atom from one to another site for higher activation energy for diffusion in HEAs, leading to sluggish diffusion. It was argued that an atom may get trapped at a low LPE site leading to sluggish diffusion (Figure 2). In HEAs, each element has a different diffusional rate, since elements with higher melting point are less active than others and thus have lower success rate for movement of the atoms. Another important contribution is due to the presence of atoms of an element with higher melting point and higher activation energy for diffusion, slowing down the overall kinetics of phase transformation which involves cooperative movement of the atoms[19].

Despite the initial enthusiasm about the sluggish diffusion effect, recent research has shown evidence of enhanced diffusion in some HEAs[20,21]. Detailed diffusion couple experiments on quaternary and quinary alloys have shown that cross terms for coefficients of the diffusivity terms arising out of the effect of one element on diffusion rate of other element play important role in diffusion. Sluggish diffusion is therefore considered as a kinetic parameter for HEAs, helping in explaining high temperature stability and presence of nanocrystalline second phase, rather than a universal effect on high entropy universe. Vaidya *et al.*[20] carried out a series of studies on tracer diffusion experiments on subset alloys of the Cantor family to show that diffusion need not necessarily be sluggish in HEAs. Their work showed that the high configurational entropy in HEAs is not necessarily responsible for sluggish diffusion.

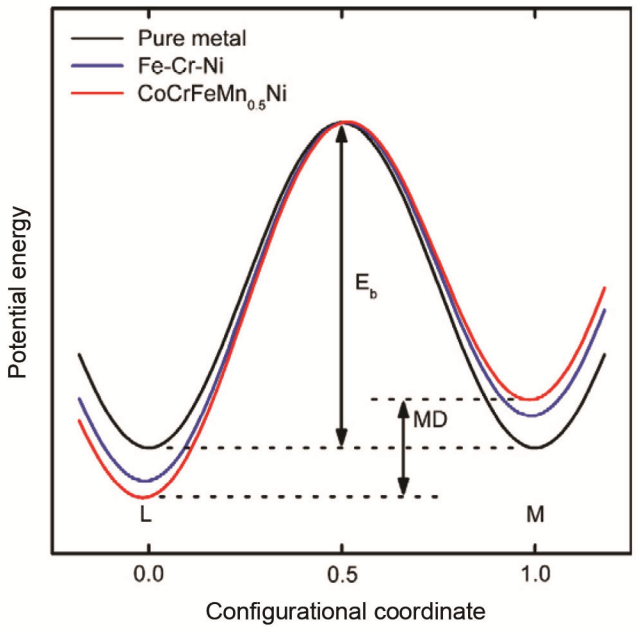

Figure 2. Schematic diagram showing the changes in lattice potential energy (LPE) during the migration of Ni atom. The molecular dynamics (MD) in potential energy for pure metals is zero, whereas that for HEAs is the largest (from ref. 88).

Severe lattice distortion: The presence of five or more atoms of different sizes present in HEAs are expected to be randomly distributed in the crystal lattice according to probability of occupancy obtained by statistical averaging. Along with different atomic sizes, different crystal structures and atomic bonding energies among asymmetrical neighbouring atoms, i.e. asymmetrical bindings and electronic structure around an atom cause severe lattice distortion than that in the traditional alloys with similar neighbourhood[22]. Figure 3 shows severe lattice distortion of a five-component BCC lattice.

The presence of sharp X-ray peaks and not-so-significant diffuse scattering indicates that there is long-range order; however, it is considered that there is localized severe lattice distortion due to difference is size of the atoms. This observation puts a question mark on the presence of this effect and it is generally accepted that only localized lattice distortion is observed in HEAs. Nevertheless, synchrotron diffraction experiments and density functional theory-based calculations have shown that individual atoms are displaced from their location by different amounts causing large local lattice distortion, but the mean distortion throughout the lattice is not significant.

Cocktail effect: The term 'multimetallic cocktails' was first mentioned by Ranganathan[23] to emphasize the unique behaviour of a mixture of elements compared to that of individual elements in bulk metallic glasses, super-elastic and super-plastic metals, and HEAs. Over time, the cocktail effect has been used to highlight the synergistic effect due to addition of multiple elements to achieve extraordinary properties that cannot be explained by conventional rule of mixtures in the aforementioned alloys, but has been one of the major effects attributed to HEAs. Ranganathan proposed that HEAs violate the rule of mixtures for composites, providing an upper bound estimate of averaging the property under consideration. He proposed that the properties of HEAs may not be an average but completely different, just like the taste of a cocktail is different from the constituent drinks. The unexpected physical properties of HEAs can be attributed to the complex structure of the alloys that opens up new property space from the available palette of elements that were inaccessible in conventional alloys. Mechanical

properties such as ultrahigh strength with sufficient ductility, high fracture toughness at cryogenic temperature, excellent fatigue and creep resistance beyond the range of conventional metals and alloys have been included in the cocktail effect. For example, addition of FCC aluminium to FCC Cantor alloy leads to destabilization of the FCC phase and a BCC phase is stabilized leading to a FCC + BCC microstructure from ~11 to 35 at% aluminium, after which a BCC phase is stabilized (Figure 4). Similarly, unique physical and functional properties like near-zero thermal expansion coefficient, catalytic, magnetic properties, photovoltaic and thermo-electric response can be considered as cocktail effect. This synergy in properties of HEAs is attributed to the evolution of complex chemistry, their microstructure and electronic structure, distinctly different from that of conventional metals and alloys.

Classes of high-entropy materials

In addition to HEAs, the family of HEMs has been broadened to include oxides[24], borides[25], nitrides and sulphides, and bulk metallic glasses[26,27]. Rost *et al.*[28] first showed entropic stabilization of five different cations in equiatomic ratios into a single-phase oxide system, opening up the entropy-stabilized solid solutions beyond metallic materials. A new terminology of 'high-entropy oxides' (HEOs) similar to HEAs was coined subsequently, that constituted oxides in the central regions of multinary oxide phase diagrams. The presence of entropy-stabilized HEOs is particularly surprising as enthalpy-dominated phase separation is a common feature of oxide phase diagrams[28]. Unlike HEAs, HEOs are characterized by random arrangement of cations of different valencies, while the oxide ions retain their sub-lattice. One of the first studied composition was (CoCuMgNiZn)O with a rock-salt structure having only one Wyckoff position for the cation[29]. With time fluorite, perovskite and spinel-based HEOs were developed. It is to be mentioned here that unlike rock salt or fluorite structure, perovskite and spinel structures have more than one Wyckoff position for the cations. Nevertheless, corresponding HEOs can be formed by replacing one or both Wykoff sites of the cation. For instance, the six-cation perovskite HEO $(Gd_{0.2}La_{0.2}Nd_{0.2}Sm_{0.2}Y_{0.2})MnO_3$ has only one site (A site) replacement in the generic ABO_3 structure, while the ten-cation perovskite $(Gd_{0.2}La_{0.2}Nd_{0.2}Sm_{0.2}Y_{0.2})(Co_{0.2}Cr_{0.2}Fe_{0.2}Mn_{0.2}Ni_{0.2})O_3$ has site replacement at both the cation sites and is characterized by an orthorhombic structure[30]. The above two examples clearly indicate the complex chemistry possible with HEOs and truly represent the complex structure of HEMs. Detailed microstructural analysis using transmission electron microscopy and X-ray absorption fine structure has revealed that there is no clustering and despite their complex structure, the oxides are truly random solutions at the atomic level. Sarkar *et al.*[31] also carried out experiments to unequivocally establish entropy-dominated stabilization of HEOs by heat treatment on HEOs at different temperatures. Rock-salt HEOs like (CuCoMgNiZn)O that show reversible transformation from a multi-phase structure (demixing of oxides) due to heat treatment at low temperature regain single-phase structure at high temperature (1000°C), forming a subset of entropy-stabilized HEOs. In addition, analogous to medium-entropy alloys, medium entropy oxides with less than five cations are also reported in the literature, thus broadening the applicability of thermodynamics-based definition of HEMs according to the enthalpy of mixing and configurational entropy of mixing[32]. The unique chemistry of HEOs leads to multi-functional behaviour that includes a combination of dielectric, magnetic, thermal and catalytic properties in a single HEO like (CoCuMgNiZn)O. Similarly, high Li-ion conductivities along with high Li-storage capability make rock salt-based HEOs a candidate battery material. In addition, the concept of entropy stabilization can be used to provide oxides suitable for thermo-mechanical processing as well as to obtain metallic to semi-conductor behaviour, providing access to functional property space beyond the scope of conventional oxides. Like conventional

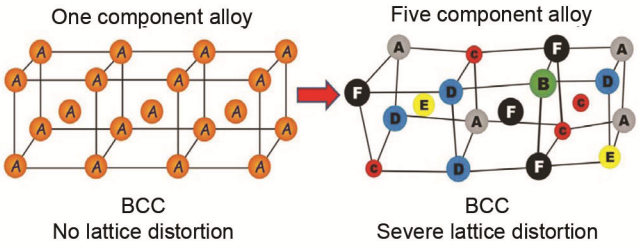

Figure 3. Schematic diagram of a five-component BCC lattice showing severe lattice distortion (from ref. 89).

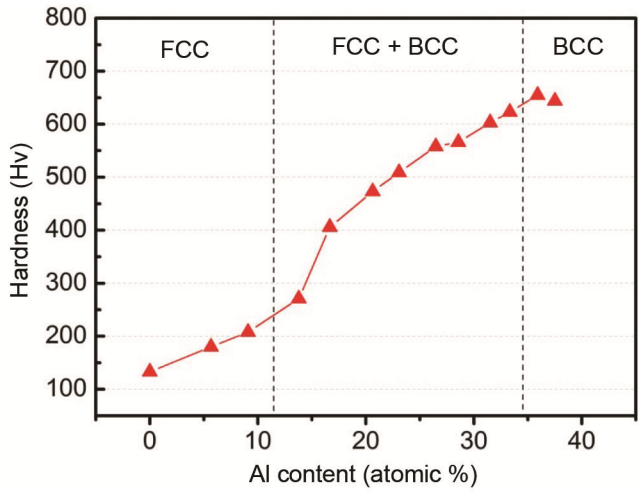

Figure 4. Cocktail effect introduced by the interaction of constituent elements in the $Al_xCoCrCuFeAl$ alloy and the corresponding variation in hardness values as a function of Al content (from ref. 87).

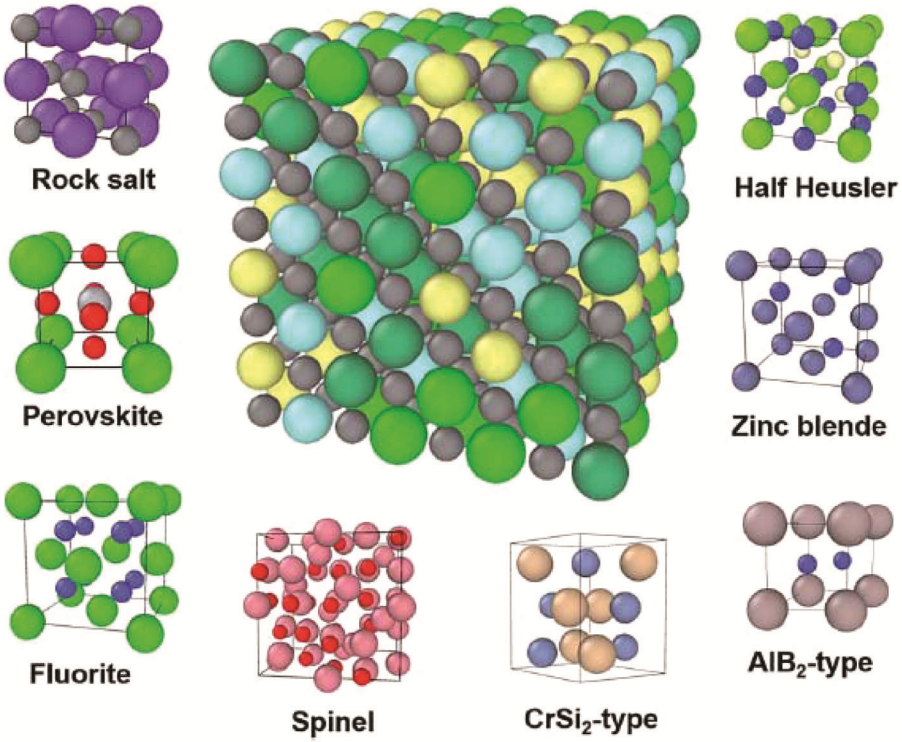

Figure 5. Structural diversity of HECs with the central image showing supercell of rock-salt structure with dark grey anions and random cations of different colours (from ref. 90).

ceramics, HEOs can be produced by the sintering route and even extremely sophisticated fabrication processes like molecular beam epitaxy can be employed to obtain epitaxial films of RHEOs for functional applications. Similarly, the ability to tailor the lattice parameter opens up a completely new avenue for obtaining multifunctionality in thin-film refractory high entropy oxide (RHEOs)[33]. In addition to oxides, carbides, borides and diborides have also shown the presence of corresponding high-entropy counterparts by cationic replacement. It has been shown that they offer better wear resistance and thermal shock resistance to conventional carbides and borides respectively. Castle *et al.*[34] successfully fabricated high-entropy carbides using ball milling and spark plasma sintering with more that 99% theoretical density at room temperature. There is some phase separation at room temperature indicating miscibility gap between the constituent carbides, but the composition shows 30% higher hardness than the hardest known binary carbides, thus opening up a new property space for hard ceramics. Gild *et al.*[35] developed six high-entropy metal diborides using high-energy ball milling followed by spark plasma sintering. These high-entropy diborides have ultrahigh melting temperature, excellent thermal and electrical conductivities, hardness, wear and oxidation resistance that are comparable and, in few cases, better than the constituent metal di-borides. Figure 5 shows the structural diversity in HECs.

Phase formation and selection

The stability of a phase in a single or multicomponent system is decided by minimization of Gibbs free energy under constant pressure, temperature and composition and is best depicted using phase diagrams. A binary phase diagram depicts phase space as a function of composition and temperature at constant pressure, while a ternary phase diagram is represented in terms of compositional space as an equilateral triangle in 2D for constant temperature and pressure. A quaternary phase diagram with four components (N) can be represented in three ($N-1$) dimensions for constant temperature and pressure as a regular tetrahedron. The four vertices represent the four components, the four faces the limiting ternary diagrams and the six edges represent the limiting binary diagrams. This analogy can be further extended to quinary phase diagrams which are of interest in the present discussion on HEAs. It can be appreciated that a five-component phase diagram can be represented in four dimensions with five vertices and five three-dimensional tetrahedra for the remaining four elements along with ten edges with limiting binary phase diagrams and ten two-dimensional boundaries with limiting ternary phase diagrams. Another important aspect is the distance of the equiatomic compositions from the single components and other higher dimensional boundaries. For instance, in a ternary phase diagram, the equiatomic composition is

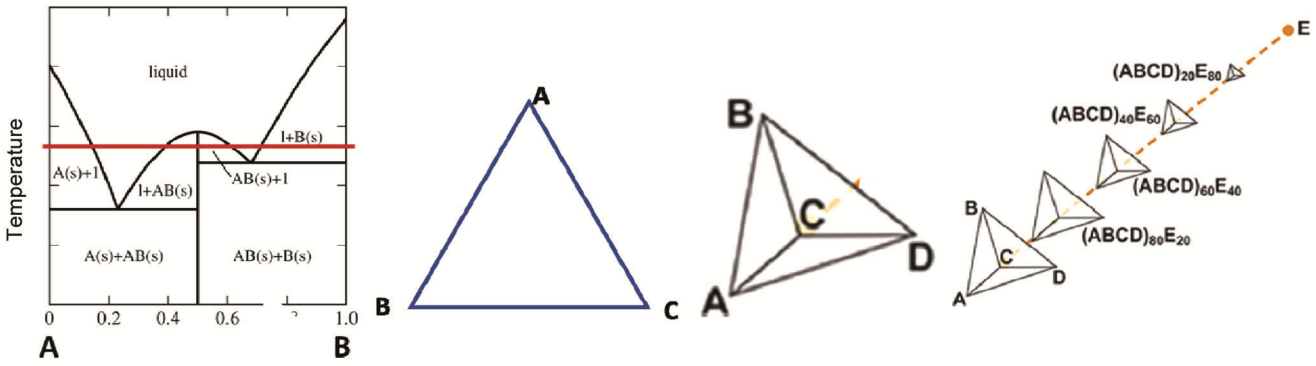

Figure 6. Isotherm in binary (red line), ternary (equilateral triangle), quaternary (tetrahedron) and quinary (series of tetrahedra diminishing in size) system depicting the complexity of the phase diagram with increase in the number of components[1,7].

67% away from the three components at the vertices and 33% away from equiatomic binary composition at the edges. The aforementioned analogy can be extended to higher (N) dimensional phase diagrams and one can realize that the equiatomic compositions become more distant from the vertices comprising single components (75% for quaternary) but less distant from the $N-1$ dimensional ternary faces (2.5% away). Though it is mathematically possible to determine the location of equiatomic composition from the limiting sub-dimensional boundaries, visualization of the same is difficult. This issue is further compounded by the spiky nature of higher-dimensional phase diagrams and concepts of terminal solutions from binary and ternary phase diagrams cannot be extended to quinary phase diagrams of HEAs. The increasing complexity in visualizing phase diagrams with increase in the number of components is depicted in Figure 6 by showing a simple isotherm in a binary, ternary, quaternary and quinary system.

The stabilization of solid solutions in HEAs appears counterintuitive to basic physical metallurgy principles, as one would expect solid solutions to be associated with terminal solid solubility and not in the central region of the phase diagrams that are generally populated with intermetallics in binary and ternary systems. However, it is to be mentioned here that unlike conventional solid solutions that are composed of solutes with solvent, it is difficult to define a solute and solvent in HEAs as all the constituent elements are present in equal or near-equal proportions. The formation of simple FCC or BCC solid solutions in these multi-principal element alloys also appears to go against the Gibbs phase rule, and the number of phases formed is much lower than that predicted. The formation of multiprincipal element solid solution in HEAs is explained on the basis of the so-called maximum entropy prediction principle proposed by Martyushev[7,36]. Intermetallics that are generally ordered phases are characterized by low entropy with stoichiometric intermetallics having zero entropy in contrast to solid solutions having high configurational entropy. It is argued that in multiprincipal element alloys, the high entropy of mixing extends the solubility limits of solid solutions enabling their formation at higher concentrations in HEAs.

Design philosophy

The aforementioned philosophy has led to the evolution of parametric approaches for the prediction of HEAs at the beginning and were followed with scientifically rigorous thermodynamic modelling strategies as well as computational methods at different length- and time-scales. A brief overview of the major strategies is given below.

Parametric approach: The crucial role of thermodynamic parameters like enthalpy and entropy of mixing, and their relative contributions to Gibbs free energy in deciding phase stability have led to various parametric approaches for predicting formation of solid solutions[37]. Parametric approaches for predicting solid-solution formation in binary systems are well established under the paradigm of Hume–Rothery rules.

- Solute and solvent elements should have similar crystal structure.
- Similar electronegativity of solute and solvent.
- Difference in the atomic diameter of solute and solvent ≤15%.
- The two elements should have similar valence. Lower valence element dissolves more in higher valence element.

On similar lines, various approaches considering atomic size difference, and difference in electronegativity are available for HEAs[38,39]. In multicomponent HEAs, the concept of solute and solvent cannot be established because of the similar concentration of elements with vastly different atomic sizes leading to severe lattice distortion. The effect of the atomic-size differences in a

Table 1. Criteria for the formation of simple solid solutions in multicomponent high-entropy alloy systems

Thermodynamic parameter	ΔH_{mix} (kJ/mol)	ΔS_{mix} (J/K mol)	δ (%)	Ω	Reference
Simple solid solution	$-20 \le \Delta H_{mix} \le 5$	$12 \le \Delta S_{mix} \le 17.5$	6.4	–	39
	–	–	≤6.6	≥1.1	40
	$-22 \le \Delta H_{mix} \le 7$	$11 \le \Delta S_{mix} \le 19.5$	$0 \le \delta \le 8.5$		95
	$-11.6 < \Delta H_{mix} < 3.2$		≤6.6		96
	$\Delta H_{mix} \ge 8.8$		≤2.77		97

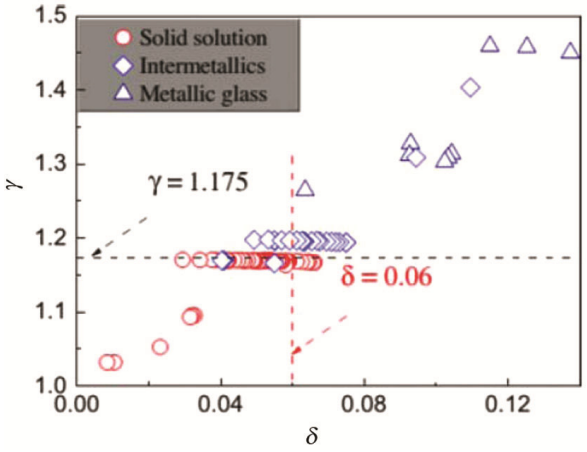

Figure 7. Comparison of γ and δ for distinguishing solid solutions from intermetallic compounds and metallic glasses (from ref. 38).

n-element alloy is described in comprehensive manner by parameter δ (ref. 39)

$$\delta = 100\left[\sum_{i=1}^{n} C_i\left(1-\frac{r_i}{r}\right)^2\right]^{1/2}, \quad \bar{r} = \sum_{i=1}^{n} C_i r_i, \tag{1}$$

where c_i is the atomic percentage of the ith component, $\bar{r}$ the average atomic radius and r_i is the atomic radius of the ith component. The enthalpy of mixing which is determined by eq. (2) is used in combination with the ó parameter to predict solid-solution formation, while Yang and Zhang[40] proposed a new dimensionless parameter omega to predict HEA phase formation along with the δ parameter. Table 1 depicts the selection rules from the aforementioned analysis.

Another parameter, mismatch entropy ($\Delta S_\sigma / k_B$) formulated by Mansoori *et al.*[41] and Raghavan *et al.*[42], was also used for prediction of high-entropy phases. Raghavan *et al.*[43] suggested that for most of the equiatomic solid solutions, $\Delta S_{config}/\Delta S_{fusion} > 1$, where ΔS_{fusion} $(= \sum_{i=1}^{N} \Delta S_{f,t})$ is the weighted average entropy of fusion for all constituent alloying elements. The $\Delta S_{f,t}$ are entropy of fusion values for individual elements in the alloy. In addition to the thermodynamic and atomic size factor, approaches based on difference in electronegativity of constituent elements and their valence electron concentrations have also been developed. For the HEA system consisting of five or more principal elements, the electronegativity difference $\Delta\chi$ has been defined as[38]

$$\Delta\chi = \sqrt{\sum_{i=1}^{n} C_i(\chi_i - \bar{\chi})^2}, \tag{2}$$

where $\bar{\chi} = \sum_{i=1}^{n} C_i\chi_i$ is the averaged electronegativity, and χ_i is the Pauling electronegativity for the ith element. Wang *et al.*[44] proposed a new geometric parameter, γ, by considering the atomic size effect based on atomic packing behaviour in HEAs. For both the solid solutions and intermetallics, γ performs much better than atomic size mismatch parameter δ, which takes the average effect of the differences in the atomic sizes of all elements in the alloy. In order to reveal the atomic packing misfit and topological instability, the ratio between the solid angles around the smallest and largest atoms with respect to the surrounding atoms is described by the geometrical parameter γ as

$$\gamma = \left(1-\frac{\sqrt{r_S + r^2 - r^2}}{(r_S + r)^2}\right) \Bigg/ \left(1-\sqrt{\frac{(r_L + r^2) - r^2}{(r_L + r)^2}}\right), \tag{3}$$

where r_S and r_L are the atomic radius of the smallest and largest atoms respectively and $\bar{r}$ is given by eq. (1). The gamma parameter performs better than the delta parameter as it can separate high-entropy solid solution phases from intermetallics and metallic glasses (Figure 7).

Integrated computational materials engineering and materials genome initiative: The integration of materials information represented in computational tools with engineering product performance analysis and manufacturing process simulations is termed as integrated computational materials engineering (ICME)[45]. The fundamental paradigm of ICME is to integrate science and engineering of materials based on theory, experiments and simulations that exist across different length- and timescales into computational tools for developing new products and manufacturing processes. A sound understanding of the theoretical aspects of experiments and computational tools is essential for the success of the ICME approach that involves bridging of length- and timescales. This involves the use of computational tools for prediction of electronic structure, atomistic structure, microstructure,

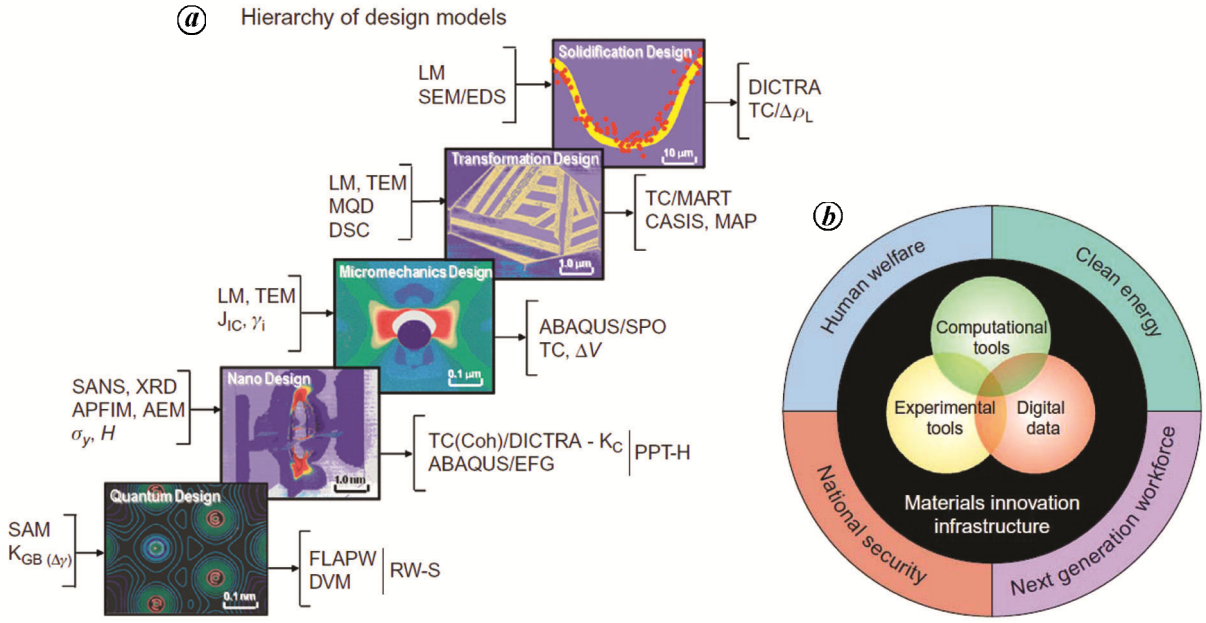

Figure 8. ***a***, Multiscale modelling framework showing the computational models and experimental tools available at different length- and timescales (from ref. 91). ***b***, Key components of the Materials Genome Initiative infrastructure and areas of application (from ref. 46).

mesostructured and continuum using tools like first principle, Monte Carlo, molecular dynamics, phase field, crystal plasticity and finite element methods (Figure 8 *a*).

The materials genome initiative (MGI) was launched by USA in 2011 to accelerate the discovery[46], development and commercial production of materials for various engineering applications[47,48]. It is expected that MGI would reduce the incubation time from discovery of a new alloy to its commercial production from the current 10–20 years or more, to a relatively short time at a sufficiently lower cost. Both ICME and MGI approaches, which are complementary to each other, have been applied to conventional alloys and there has been an impetus to employ the same strategy towards accelerated development of HEAs. Figure 8 *b* shows the major constituents of the MGI framework.

CALPHAD: CALculation of PHAse diagrams (CALPHAD) approach is a thermodynamic modelling tool that includes Gibbs free energies of different phases as a function of temperature and composition for various binary and ternary alloy systems from experimental and theoretical results[49,50]. The tool provides a thermodynamic language for analysing different alloy systems that can be used to predict the evolution of phases based on the principle of minimization of Gibbs free energy. It also offers a methodology to obtain information of higher-order systems from lower-order systems; for instance, phase stability for a ternary composition at constant temperature and pressure can be predicted by considering the corresponding binary and uniary alloy systems. Various Gibbs free energy minimizer codes like Thermo-Calc append the data of lower-order systems to describe higher-order systems and map the equilibrium states for different thermodynamic conditions, including those which data are not available. This methodology can be extended to quinary HEAs, which makes the CALPHAD one of the most potent approaches to predict phase stability in HEAs. In order to achieve high-fidelity predictions, the database used to determine phase stability has to be robust, and over the years CALPHAD has evolved from databases for aluminium, titanium and iron alloys to name a few to actual HEA databases HEA1 and HEA3 that constitute Gibbs free energy data for different ternary, quaternary and quinary systems for transition metal HEAs. Figure 9 *a* is a block diagram demonstrating the phenomenological approach employed by CALPHAD to predict thermodynamic description of a multicomponent system including HEAs for which thermochemistry data are unavailable in a self-consistent manner. Figure 9 *b* shows the extrapolation of higher-order phase diagram from lower-order phase diagrams.

In one of the early studies, Gao and Alman[51] explored phase stability in 16 multi-component systems for single-phase HEAs and extended their approach to unearth FCC and HCP HEAs. Other researchers, studied phase stability in 130,000 equimolar compositions from a palette of 45 elements based on high-throughput computation and simple rules to explore the potential of the alloy for structural applications based on phase characteristics, their transformation temperature, and rough estimation of alloys microstructure-insensitive properties. Tazuddin *et al.*[52] have effectively utilized the Thermo-Calc software to study the effect of composition on phase evolution by

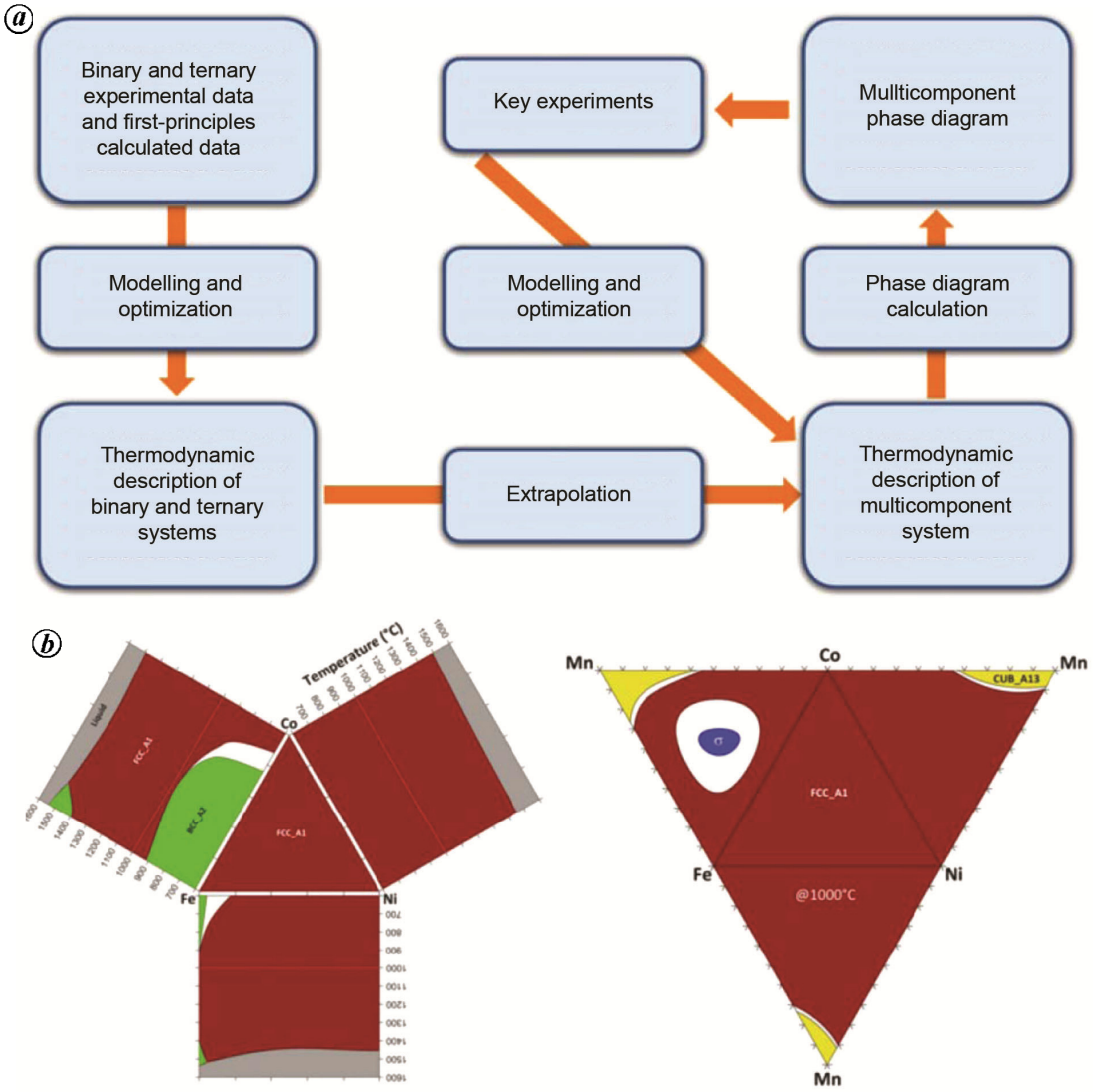

Figure 9. ***a***, Schematic diagram showing the phenomenological approach used to obtain thermodynamic description of multicomponent systems in CALPHAD. ***b***, Calculated subcomponent binaries along with a ternary isotherm for the Co–Fe–Ni system (left) and unfolded tetrahedron of Co–Fe–Ni–Mn system (right) at 1000°C (from ref. 92).

varying all constituent elements of CoCuFeMnNi from 5 to 35 at% using aluminium, iron and titanium database. The modelling resulted in unearthing ten single-phase equiatomic compositions from the 1287 compositions available from the 13 elements for all the three databases, albeit with minor difference in the phase fields at different temperatures. However, experimental observations showed that only 6 out of 10 compositions predicted by CALPHAD were single-phase. Sonkusare *et al.*[53] used the TCHEA1 and TCHEA3 databases to determine the pseudo-binary phase diagram for the CoCuFeMnNi HEA, and explain the evolution of phases with temperature using *in situ* high-temperature X-ray diffraction. Recently, Raturi *et al.*[54] have performed CALPHAD modelling to develop non-equiatomic refractory HEAs from refractory elements in the periodic table using TCHEA3 database coupled with state-of-the-art characterization and high-throughput instrumented indentation experiments. The qualitative prediction of phase fraction in multi-phase HEAs offers a unique tool to establish their microstructure property paradigm. Thus, it has been expected that these techniques will offer immense scope for design and development of an enormous number of HEAs in the future. There is focus on goal-oriented HEA development, and HEA systems based on the presence of B2 intermetallic phase for high-temperature strength, precipitation hardening and even obtaining twinning and/or transformation-induced plasticity by engineering stacking fault energy in FCC HEAs have been attempted with reasonable success.

Ab initio methods: *Ab initio* or first-principles quantum chemistry methods are designed to solve the electronic structure using Schrödinger equation for a system comprising nuclei located at a specific position with a

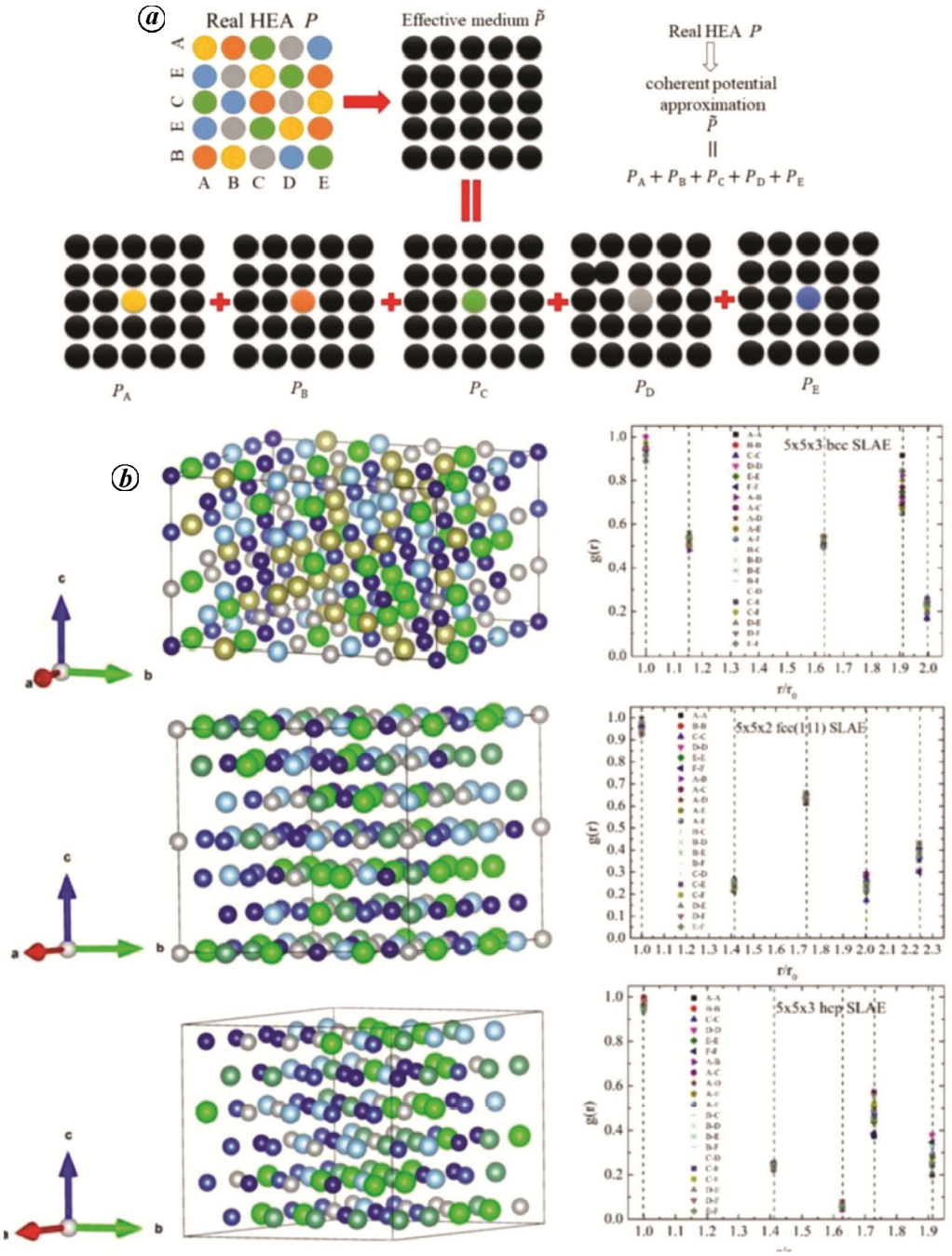

Figure 10. ***a***, Illustration of two-dimensional coherent potential approximation to ABCDE HEA, where *P* represents the alloy potential and *P* with subscript indicates the potential of individual elements. ***b***, Structural illustration (left) and radial distribution function (right) for ABCDE HEA with BCC, FCC and HCP structures (top to bottom; from ref. 93).

number of electrons to provide information on electron densities, energies and other microstructure-insensitive properties like elastic modulus, coefficient of thermal expansion, theoretical shear strength and generalized stacking fault energy of the alloy system. Density functional theory (DFT) in which the multi-electron Schrödinger equation is mapped into an effective one-electron problem utilizing electron density as an important variable in the Kohn–Sham approximation and *ab initio* molecular dynamics (AIMD) have been developed to solve the potential of the system in the ground state. The application of different *ab initio* methods is challenging for HEAs due to the large number of atoms involved and uncertainty in the location of individual atoms[55]. For conventional solid-solution alloys, supercell approximation of periodic boundary condition is artificially imposed on supercell of sufficiently large size to capture the chemical disorder of the system and study the disordered configuration.

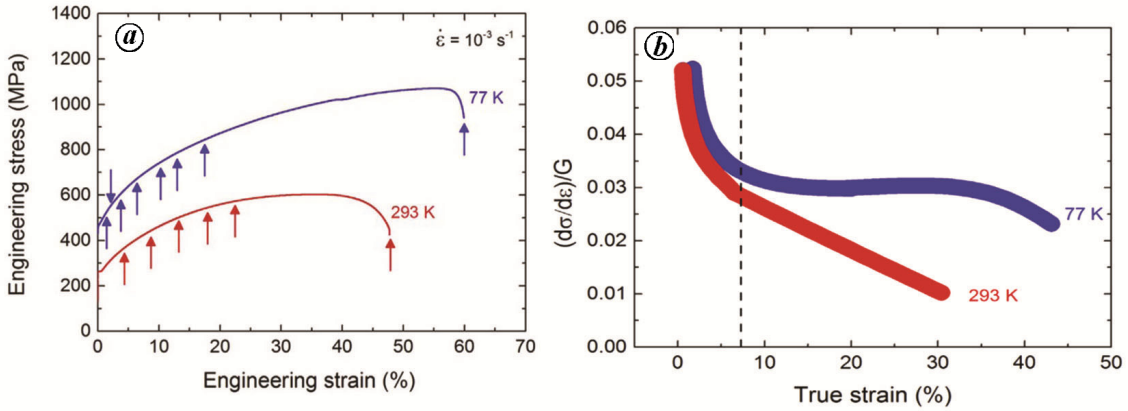

Figure 11. (***a***) Engineering stress–engineering strain and (***b***) strain hardening–true strain curves for CoCrFeMnNi HEA tested at room temperature and cryogenic temperature (from ref. 57).

Ab initio calculations for HEAs utilize the virtual crystal approximation or coherent potential approximation using a supercell with random or quasi-random atomic distribution. Another method is to introduce the concept of homogeneous effective medium that uses a primitive periodicity cell to study the arbitrary chemical disorder. Figure 10 *a* shows a two-dimensional illustration of CCA for ABCDE equimolar HEA and the strategy to determine the potential of the HEA from individual atomic potentials. Figure 10 *b* is a schematic of a supercell of 150 atoms with similar local atomic environment for equimolar ABCDE HEA for BCC, FCC and HCP structure (left) and the corresponding radial distribution functions (right).

A detailed review of different *ab initio* methods for HEAs is provided by Ikeda *et al.*[56], wherein a detailed account of *ab initio* studies on HEAs to analyse various properties like short-range ordering, stacking fault energy, lattice distortion, diffusion, phase stability as well as elastic and magnetic properties is provided.

Properties of high-entropy alloys

Mechanical properties of high-entropy materials

A host of mechanical properties like elastic modulus, tensile and compressive yield strength, toughness and fracture toughness have been studied for HEAs over a wide range of temperature and strain rate. In addition, fatigue, creep and fracture properties have been studied for a variety of HEAs. The most widely studied alloy is the equiatomic CoCrFeMnNi (Cantor) alloy showing low yield strength but high strain hardening ability at room temperature. The elastic modulus of the alloy increases with decrease in temperature from 300 to 77 K, similar to that of FCC nickel albeit with a slightly lower temperature dependence, while it decreases with increase in temperature above room temperature. The yield strength and tensile strength increase with decrease in temperature from 273 to 77 K (Figure 11 *a*), accompanied by monotonic increase in elongation with decrease in temperature[57]. Detailed TEM studies have shown that octahedral slip is operative at yielding over the wide temperature range with presence of planar ⟨110⟩ dislocation and numerous stacking faults. The presence of planar dislocations was attributed to destruction of short-range ordering or clustering, or operation of partial slip inhibiting cross slip in FCC materials. There is formation of dislocation cell structure at higher strains at room temperature and above, while nanoscale twinning was observed at 77 K for strain of 20%. The change in elastic modulus with temperature cannot explain the variation in yield strength at cryogenic temperature; the alloy shows higher strength and ductility due to operation of twinning providing additional strain hardening (Figure 11 *b*) due to dynamic Hall–Petch effect[58]. The evolution of yield strength in Cantor alloy can be explained on the basis of different strengthening mechanisms like solid-solution strengthening, grain-size hardening and strain hardening. Hall–Petch hardening has a weak dependence on temperature and strain rate, while the latter two are strain rate and temperature-dependent, while strain hardening is also dependent on strain. The activation volume of Cantor alloy at room temperature is $300b^3$ and decreases to $25b^3$ at 77 K, indicating that reduction in mean free path for dislocations is the rate-controlling mechanism. Though the activation volume is lower than that of pure FCC metals, it is comparable to that of solid solution and a decrease in activation volume with increase in strain or decrease in temperature indicates that no new intrinsic deformation mechanisms are operative in FCC Cantor alloy. Komarasamy *et al.*[59], however, showed that activation volume of coarse-grained $Al_{0.1}$CoCrFeNi HEA was lower than that of conventional FCC materials, and this was attributed to intrinsic lattice distortion of HEAs compared to that of FCC metals and alloys. It was proposed that the dislocation line energy and Peierls potential in HEAs may have a continuous variation contrary to constant line energy and

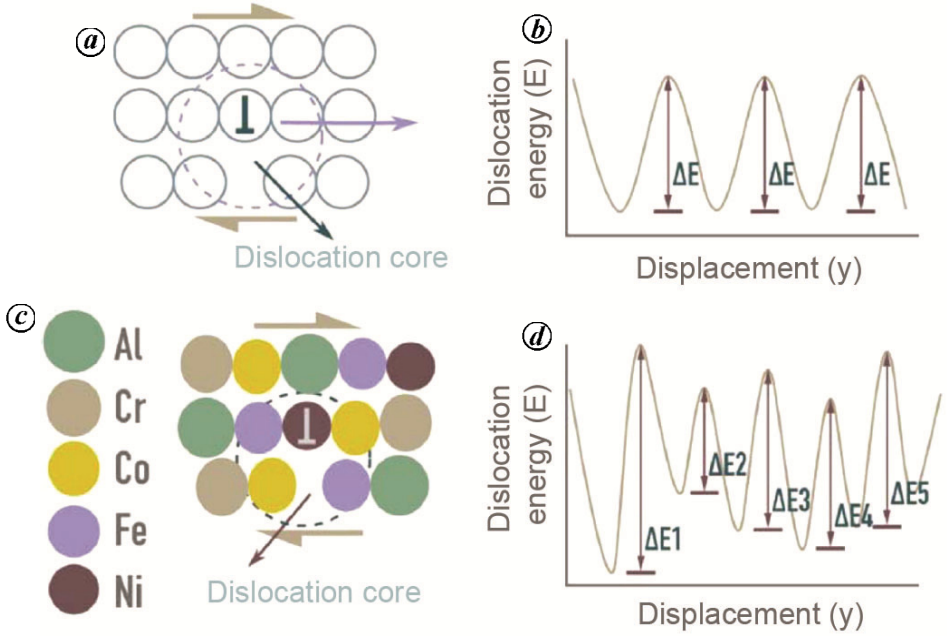

Figure 12. ***a***, ***b***, Edge dislocation in a pure (***a***) metal with corresponding dislocation energy with movement (***b***). ***c***, ***d***, Edge dislocation in AlCoCrFeMnNi HEA (***c***) with corresponding dislocation energy with displacement (***d***) (from ref. 59).

potential in conventional alloys. The presence of varying potential barrier offers a unique environment for dislocation movement with the deep wells acting as dislocation pinning points in the lattice. This leads to smaller length of dislocation involved in thermal activation and to lower physical activation volume. Figure 12 is a schematic comparing the dislocation structure and motion in pure metal vis-á-vis HEA.

The Cantor alloy shows exceptional fracture toughness (250 MPa $m^{0.5}$), even better than the best austenitic steels reported in the literature till date and retains it at cryogenic temperature due to twinning operation (Figure 13). *In-situ* TEM experiments also show high toughness due to crack bridging by nanotwinning (Figure 14), which further explains the exceptional damage tolerance of this alloy[58]. The operation of planar partial slip and nanotwinning across a temperature regime enthrones the Cantor alloy to the pinnacle of engineering alloys in terms of yield strength and fracture toughness (Figure 15)[60].

In addition to Cantor alloy, another class of HEAs offering excellent strength and ductility exploits strain hardening mechanisms like twinning, transformation-induced plasticity, dual phase hardening, common in steels. In a pioneering study by Li *et al.*[61], it was shown that excellent combination of strength and ductility can be obtained in a series of $Fe_{80-x}Mn_xCo_{10}Cr_{10}$ alloys that form a class of non-equiatomic HEAs by exploiting twinning-induced plasticity for lower manganese content, while transformation of FCC austenite to HCP martensite phase provides higher strain hardening with higher manganese content. The $Fe_{50}Mn_{30}Co_{10}Cr_{10}$ alloy is characterized by the presence of FCC austenite and HCP martensite phase and on further deformation, there is transformation of austenite to martensite providing transformation-induced plasticity to yield exceptional combination of strength and ductility (Figure 16). This study has motivated several others to explore multiple strengthening mechanisms in HEAs, which are not possible in a single composition of steel. Addition of interstitial carbon to these alloys has led to the evolution of HE steels and transformative HEAs offering a property space for strength and ductility that was not accessible even after 100 years of research in steels and other metallic materials (Figure 17)[62].

In addition to Cantor alloy, other single-phase HEAs like CoCuFeMnNi[63,64] have also been studied in detail, while BCC refractory HEAs have been examined with respect to in tension and compression over a wide range of temperature, viz. from room temperature to 1873 K. Tazuddin *et al.*[65] showed that CoCuFeMnNi is a single-phase FCC HEA that shows higher yield strength compared to Cantor alloy and is characterized by formation of a Goss-brass texture on cold rolling due to operation of planar partial slip. Sonkusare *et al.*[53] showed that the alloy consists of copper-rich nanoclusters of ~2.5 nm that contribute to significant strengthening. They also studied large strain behaviour of CoCuFeMnNi HEA in monotonic and cyclic high-pressure torsion to show extreme grain refinement and partial dissolution of copper-rich nanoclusters[66]. It was proposed that non-equilibrium solid-solution strengthening at high strain contributes to higher hardness of the high-pressure torsion-tested sample, in

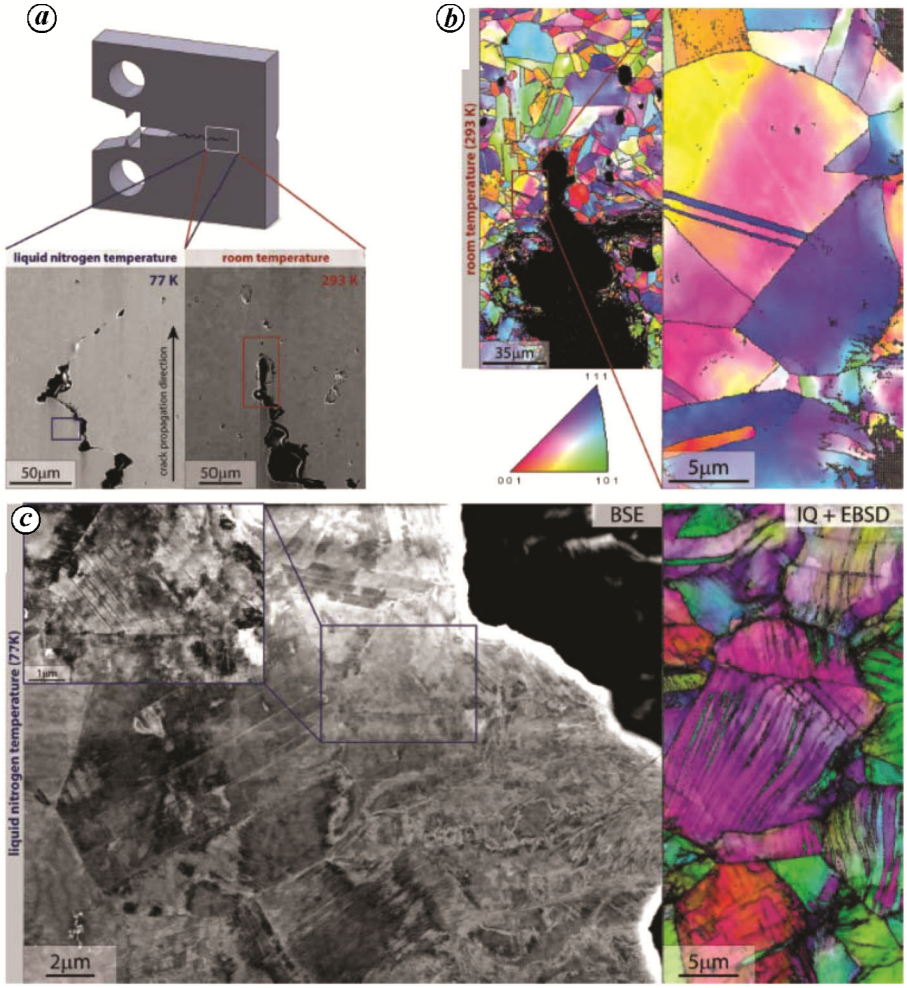

Figure 13. ***a***, Deformation mechanisms near the crack tip in CoCrFeMnNi HEA in terms of secondary image from scanning electron microscopy for the sample tested at 293 and 77 K. ***b***, EBSD inverse pole figure map showing annealing twins with large misorientations in the sample tested at 293 K. ***c***, Back-scattered electron image showing nanotwinning and cell formation in the sample tested at 77 K (from ref. 60).

addition to grain size and dislocation hardening. The refractory HEAs are potential replacement for superalloys and hence, their high-temperature mechanical properties have been studied in detail. Most single and multi-phase RHEAs have at least one disordered BCC phase and show limited ductility at room temperature under tension at room temperature. Cast and homogenized HfNbTaTiZr RHEA shows high strength in the range 800–1000 MPa and compressive ductility up to 50% over a wide temperature range from room temperature to 1273 K, while the homogenized sample shows 10% ductility in tension[67]. Senkov *et al.*[68] showed improved high-temperature compressive properties of $Nb_{25}Mo_{25}Ta_{25}W_{25}$ and $V_{20}Nb_{20}Mo_{20}Ta_{20}W_{20}$ RHEAs compared to two superalloys, Inconel 718 and Haynes 230 (Figure 18).

In addition to tensile and compressive properties, hardness is also an important material property and HEAs offer a wide range of hardness, from 150 to 1200 HV, depending on the synthesis method and type of phases and their size and distribution in the alloy under consideration. Generally, HEAs produced by ball milling and sintering route show much greater hardness than those produced by the melting and casting route while BCC HEAs show greater hardness compared to FCC HEAs. Mohanty *et al.*[69–71] have studied a series of HEAs produced by powder metallurgy route to achieve high modulus and hardness by exploiting sinter ageing as well as eutectoid transformations, while Yadav *et al.*[72–74] have reported that powder metallurgy-based HEAs show good wear resistance. The cyclic properties of HEAs in high-cycle fatigue regime[75,76] and low-cycle fatigue regime[77] show that they can outperform conventional alloys in terms of fatigue life and resistance to fracture.

High-cycle fatigue behaviour of as-cast and wrought $Al_{06.5}CoCrCuFeNi$ alloy was studied by Hemphill *et al.*[73] using four-point bending test at room temperature to establish fatigue endurance limit in the range 540–945 MPa for the present alloy system. Tang *et al.*[76]

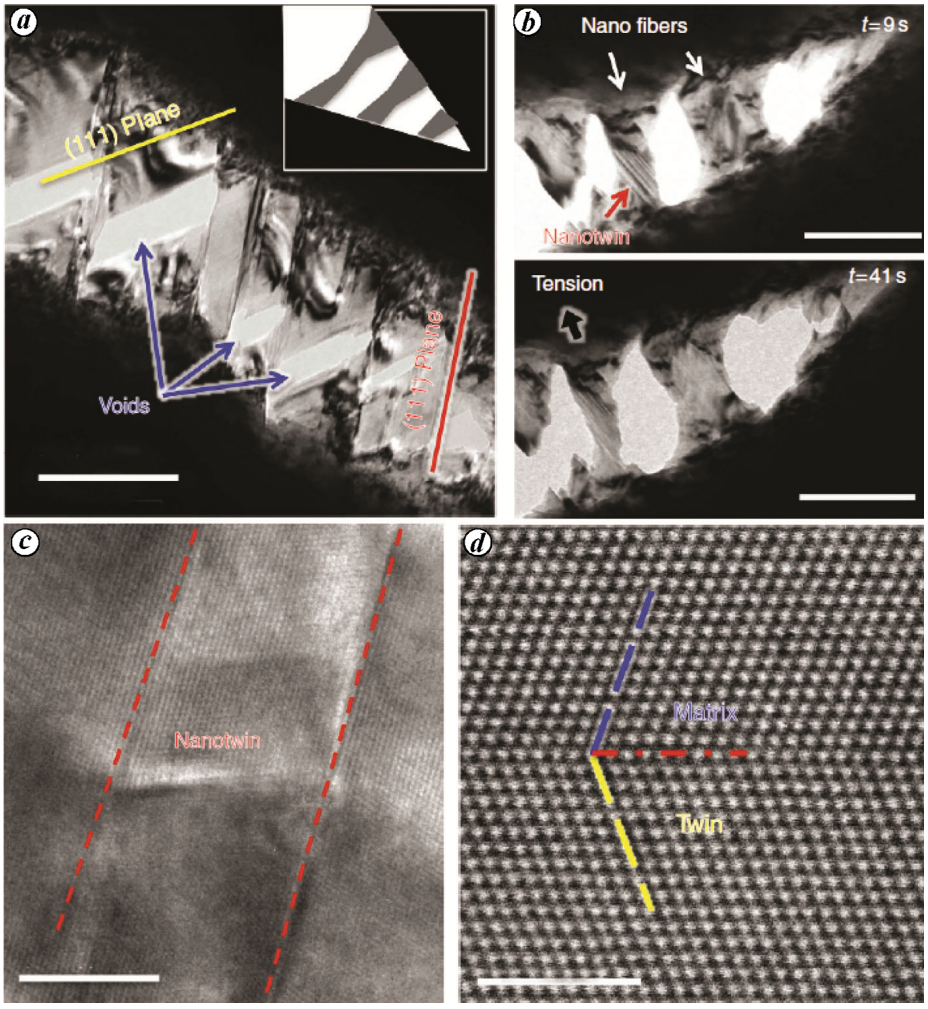

Figure 14. Collage of image showing crack bridging by near-tip twin nanobridges in CoCrFeMnNi alloy tested using *in-situ* TEM showing (***a***) bright field TEM image showing void formation, (***b***) TEM image showing bridging by formation of nanotwins, (***c***) high-resolution transmission electron microscope image showing nanotwin formation and (***d***) high angle annular dark field -TEM image showing twin (from ref. 60).

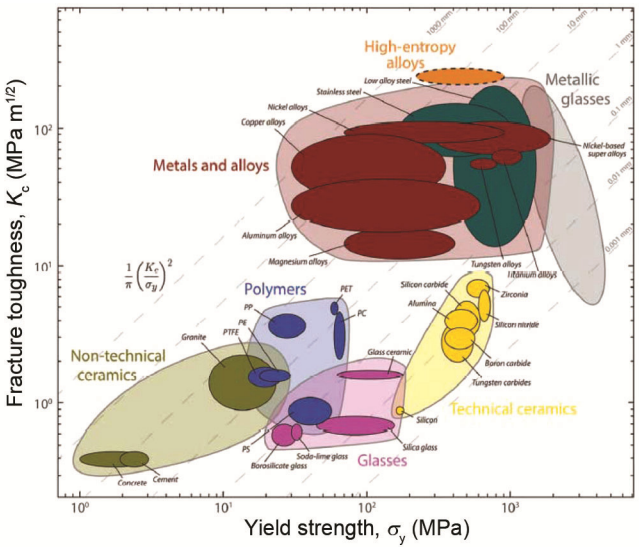

Figure 15. Ashby map for fracture toughness as a function of yield strength for engineering materials including HEAs (from ref. 60).

showed that the use of high-purity elements for synthesis of $Al_{0.5}CoCrCuFeNi$ alloy provides better fatigue performance. The higher endurance limit and prolonged fatigue life of HEA vis-à-vis conventional alloys was attributed to the absence of aluminium-oxide inclusions and microcracks in the high-purity sample along with the formation of nano-twins during cyclic loading (Figure 19). Tang *et al.*[76] and Bahadur *et al.*[77] have shown sufficient LCF performance of HEAs. Cantor alloy shows good creep resistance and can also provide superplastic deformation after grain-size reduction via high-pressure torsion[78].

Functional properties

Most studies on HEMs, particularly on HEAs, have focused on mechanical properties; however, HEAs and particularly HECs, also offer an opportunity to explore property space in the functional regime, including superior magnetic, magnetocaloric, thermoelectric, piezoelectric,

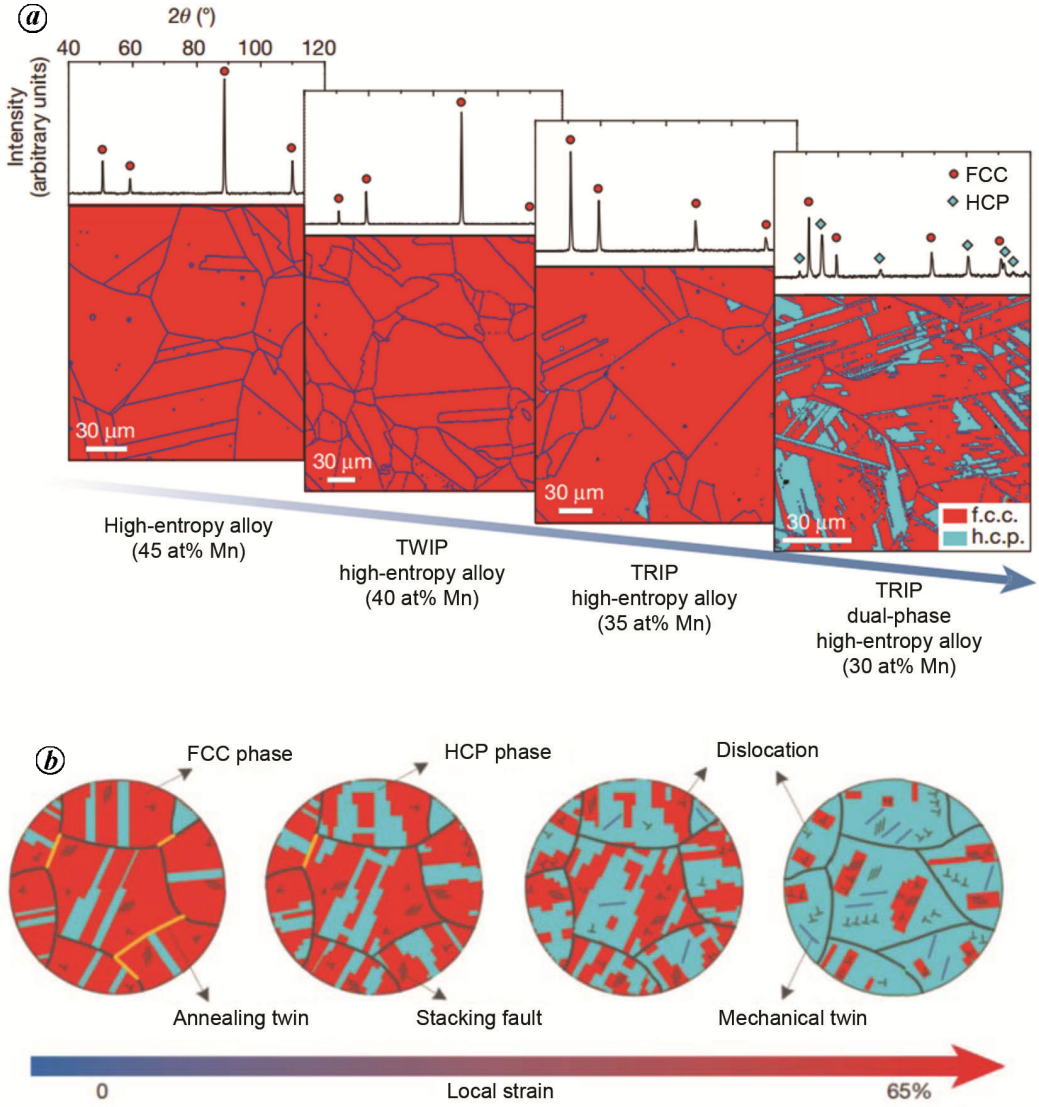

Figure 16. ***a***, Variation of microstructure with manganese content in FeMnCoCr alloys. ***b***, Deformation processes in FCC and HCP phases of 30 at% Mn alloy (from ref. 61).

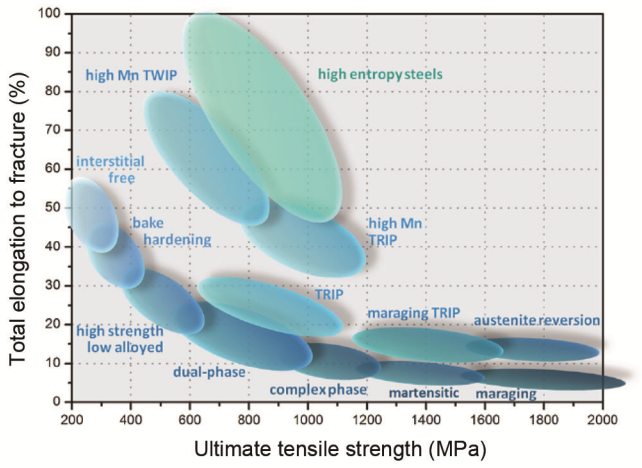

Figure 17. Ashby plot for ultimate tensile strength and total elongation showing different classes of steel, including the newly developed high-entropy steels (from ref. 94).

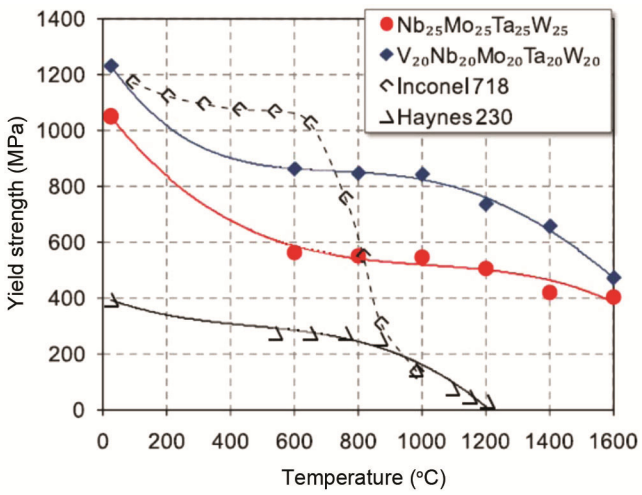

Figure 18. Variation of yield stress of BCC HEAs and two commonly used superalloys Inconel 718 and Haynes 230 (from ref. 68).

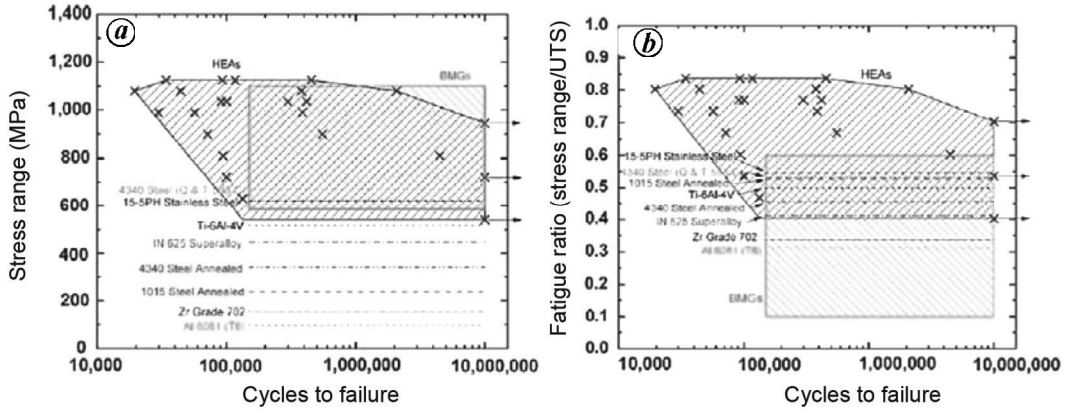

Figure 19. ***a***, Stress range versus number of cycle to failure diagram (S–N curve). ***b***, Fatigue ratio (stress range/ultimate tensile strength) versus number of cycles for $Al_{0.5}CoCrCuFeNi$ HEA and other engineering materials (from ref. 75).

multiferroic and catalytic properties. The research on functional properties of HEMs is in a nascent stage, but is bound to explode in the coming years considering the huge potential displayed by the initial studies. HEAs containing ferromagnetic elements offer low magnetocrystalline anisotropy and low magnetostriction as well as low intrinsic coercivity, low electrical resistance but high saturation magnetization. Addition of elements like aluminium and silicon to CoFeNi increases the saturation magnetization and provides HEAs with excellent mechanical strength and corrosion resistance for soft magnetic applications[79]. Multi-phase HEAs containing two or more high-entropy phases, or a combination of high-entropy phase and intermetallic or high-entropy glasses offer a wide range of soft magnetic properties for HEMs. Yuan *et al*.[80] showed that HCP DyErGdHoTb alloy has a small magnetic hysteresis and high refrigerant capacity (a figure of merit parameter for magnetoelectric effect), which is the product of magnetic entropy and temperature span of full width at half maxima (FWHM) for the entire span of the entropy curve. It was also observed that the presence of Gd is essential to obtain magnetocaloric effect. HEAs like CoCrFeMnNi[81], $Al_xCoCrFeMn$ and CoCrFeNiPd[82] showed higher resistivity than those of 316 and 304 stainless steels. Thermoelectric materials exploit the Seebeck effect that produces voltage from temperature difference between two materials possessing high Seebeck coefficient (a figure of merit) and high electrical conductivity with low thermal conductivity. A highly distorted lattice in HEAs can reduce the electron mean free path and substantially reduce electrical and thermal conductivity by orders of magnitude for single- and multiphase HEAs. Shafeie *et al*.[83] showed that with increasing aluminium content in $Al_xCoCrFeNi$ HEAs, there is an increase in Seebeck coefficient and thermal resistivity, which is beneficial for thermoelectric properties but there is a decrease in electrical conductivity which is undesired. Figure 20 depicts the thermoelectric performance of a series of HEAs in terms of power factor and efficiency.

Another important area particularly for BCC HEAs is in hydrogen storage, wherein the candidate material should be capable of absorbing and storing large quantities of hydrogen without damage and should have the ability to release it when required. Among various BCC HEAs, HfNbTiVZr[84] shows excellent hydrogen absorption which is superior to all the constituent elements, indicating that the distorted lattice in HEAs aids in hydrogen absorption at both octahedral and tetrahedral voids. Other RHEAs like $(FeV)_{0.6}(CoCrTi)_{0.4}$ and $(FeV)_{0.6}(CoCrTi)_{0.38}Zn_{0.02}Ni_{20}Fe_{20}Mo_{10}Co_{35}Cr_{15}$ also show good hydrogen storage capability[85].

The corrosion behaviour of various single- and multiphase HEAs in different corrosive environments like NaCl indicates that they show a better performance than the constituent elements of conventional alloys like austenitic steels. Similarly, HfNbTaTiZr showed spontaneous passivation at room temperature in HNO_3 and HNO_3 + NaF environment, but was severely corroded in boiling fluorinated nitric acid at 120°C. RHEAs offer an excellent oxidation resistance compared to refractory elements that have a poor oxidation resistance with alloys containing aluminium and silicon showing formation of complex but stable oxide films that provide excellent oxidation resistance.

Outstanding issues and future direction (future challenges)

HEMs have opened up a completely new compositional space as well as performance space, albeit in some cases. However, our fundamental understanding of basic thermodynamics, diffusion, physical metallurgy, mechanical, physical and functional properties is still valid for HEMs and, in fact has evolved with HEMs. Although, the underlying synergy among different mechanisms offers exceptional properties, to foe HEA. The biggest challenge is to search their composition from a large compositional

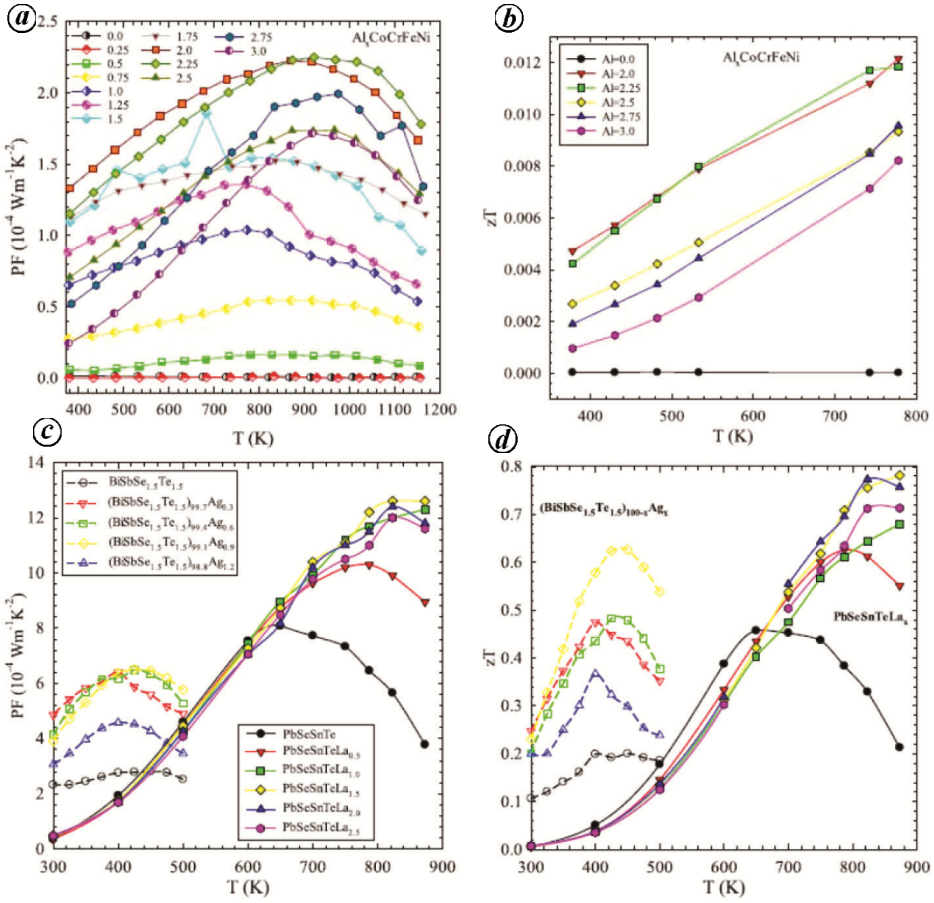

Figure 20. Variation of power factor (PF) and figure of merit (zT) with temperature for different HEAs (from ref. 83).

space. To this end, high-throughput experimental and property-driven alloy development using computational methods across length- and timescales need to be adopted and subsegment combinational synthesis will allow us to fine tune composition of these multicomponent alloys to arrive at the best properties. There is scope for development of new materials with fascinating properties. By adopting new methods for first-principles calculations, thermodynamic modelling, dislocation statics and dynamic simulations, with high-throughput experiments, a fundamental understanding of the process being operative in HEMs can unequivocally be established with process–structure–property-performance linkage.

However, several specific issues need to be resolved and we shall deliberate on a few of them. The role of local chemical order in these materials on the macroscopic properties needs to be deciphered through combination of DFT-based computer simulations and careful experiments using synchrotron diffraction. It is evident that the degree of local chemical order plays a major role on the stacking-fault twinning energy, leading to Transformation Induced Plasticity and Twin Induced Plasticity behaviour. This can open up new vistas for the design of alloys with near-zero stacking-fault energies and metastable HEAs with small stacking-fault energies; leading to deformation-driven twinning and phase transformation. The role of interstitial elements (C, O, N) on phase formation, stability and mechanical properties of HEAs needs to be fully understood[86,87]. Recent research reveals that O, although considered as 'energy' in metallic materials, can improve both strength and ductility in HfNbTiZr HEA via formation of O-TiZr-rich order clusters. Unique functional properties in this 'multi-metallic cocktail' can lead to interesting and novel applications due to magnetic, thermoelectric and catalytic properties. Multi-functionality of the multicomponent materials can lead to new processes or products, and hence, future exploration is necessary. In a nutshell, we need to pay more attention to potential innovative applications in order to keep the field active and sustained for long. Certainly the challenges listed here provide enough 'food for thought' for materials scientists and engineers in their quest of the 'holy grail of materials science'.

1. Murty, B. S., Yeh, J. W. and Ranganathan. S., *High Entropy Alloys*, Butterworth–Heinemann, Elsevier, UK, 2014.
2. Gao, M. C., Yeh, J. W., Liaw, P. K. and Zhang, Y., *High Entropy Alloys: Fundamentals and Applications*, Springer, Switzerland, 2016.
3. Yadav, S., Biswas, K. and Kumar, A., Spark plasma sintering of high entropy alloys. In *Spark Plasma Sintering of Materials:*

Advances in Processing and Applications, Springer Nature Publishers, 2019, pp. 539–571.
4. Yan, X., Constantin, L., Lu, Y., Silvain, J.-F., Nastasi, M. and Cui, B., $(Hf_{0.2}Zr_{0.2}Ta_{0.2}Nb_{0.2}Ti_{0.2})C$ high-entropy ceramics with low thermal conductivity. *J. Am. Ceram. Soc.*, 2018, **101**, 4486–4491; doi:https://doi.org/10.1111/jace.15779.
5. Zhou, J., Zhang, J., Zhang, F., Niu, B., Lei, L. and Wang, W., High-entropy carbide: a novel class of multicomponent ceramics. *Ceram. Int.*, 2018, **44**, 22014–22018; doi:https://doi.org/10.1016/j.ceramint.2018.08.100.
6. Sharma, A. S., Yadav, S., Biswas, K. and Basu, B., High-entropy alloys and metallic nanocomposites: processing challenges, microstructure development and property enhancement. *Mater. Sci. Eng.: R: Rep.*, 2018, **131**, 1–42; doi:https://doi.org/10.1016/j.mser.2018.04.003.
7. Miracle, D. B. and Senkov, O. N., A critical review of high entropy alloys and related concepts. *Acta Mater.*, 2017, **122**, 448–511; doi:https://doi.org/10.1016/j.actamat.2016.08.081.
8. Kumar, J., Kumar, N., Das, S., Gurao, N. P. and Biswas, K., Effect of Al Addition on the microstructural evolution of equiatomic CoCrFeMnNi alloy. *Trans. Indian Inst. Met.*, 2018, **71**, 2749–2758; doi:10.1007/s12666-018-1443-4.
9. Gorsse, S., Miracle, D. B. and Senkov, O. N., Mapping the world of complex concentrated alloys. *Acta Mater.*, 2017, **135**, 177–187; doi:https://doi.org/10.1016/j.actamat.2017.06.027.
10. Gorsse, S., Couzinié, J.-P. and Miracle, D. B., From high-entropy alloys to complex concentrated alloys. *C. R. Phys.*, 2018, **19**, 721–736; doi:https://doi.org/10.1016/j.crhy.2018.09.004.
11. Yeh, J. W. *et al.*, Nanostructured high-entropy alloys with multiple principal elements: novel alloy design concepts and outcomes. *Adv. Eng. Mater.*, 2004, **6**, 299–303; doi:10.1002/adem.200300567.
12. Yeh, J.-W., Recent progress in high-entropy alloys. *Sci. Mater.*, 2006, **31**, 633–648; doi:https://doi.org/10.4028/www.scientific.net/AMR.631-632.227.
13. Cantor, B., Chang, I. T. H., Knight, P. and Vincent, A. J. B., Microstructural development in equiatomic multicomponent alloys. *Mater. Sci. Eng. A*, 2004, **375–377**, 213–218; doi:https://doi.org/10.1016/j.msea.2003.10.257.
14. Li, Z. and Raabe, D., Strong and ductile non-equiatomic high-entropy alloys: design, processing, microstructure and mechanical properties. *J. Mater.*, 2017, **69**, 2099–2106; doi:10.1007/s11837-017-2540-2.
15. Mac, B. E. *et al.*, Recent progress in high entropy alloy research. *J. Mater.*, 2017, **69**, 2024–2031; doi:https://doi.org/10.1007/s11837-017-2484-6.
16. Tsai, M. H. and Yeh, J. W., High-entropy alloys: a critical review. *Mater. Res. Lett.*, 2014, **2**, 107–123; doi:https://doi.org/10.1080/21663831.2014.912690.
17. Ma, D., Grabowski, B., Körmann, F., Neugebauer, J. and Raabe, D., *Ab initio* thermodynamics of the CoCrFeMnNi high entropy alloy: importance of entropy contributions beyond the configurational one. *Acta Mater.*, 2015, **100**, 90–97; doi:https://doi.org/10.1016/j.actamat.2015.08.050.
18. Tsai, K.-Y., Tsai, M.-H. and Yeh, J.-W., Sluggish diffusion in Co–Cr–Fe–Mn–Ni high-entropy alloys. *Acta Mater.*, 2013, **61**, 4887–4897; doi:https://doi.org/10.1016/j.actamat.2013.04.058.
19. Chang, S.-Y. and Chen, D.-S., 10-nm-thick quinary (AlCrTaTiZr)N film as effective diffusion barrier for Cu interconnects at 900°C. *Appl. Phys. Lett.*, 2009, **94**, 231909; doi:https://doi.org/10.1063/1.3155196.
20. Vaidya, M., Mohan Muralikrishna, G., Divinski, S. V. and Murty, B. S., Experimental assessment of the thermodynamic factor for diffusion in CoCrFeNi and CoCrFeMnNi high entropy alloys. *Scr. Mater.*, 2018, **157**, 81–85; doi:https://doi.org/10.1016/j.scriptamat.2018.07.040.
21. Dabrowa, J. *et al.*, Demystifying the sluggish diffusion effect in high entropy alloys. *J. Alloy. Compds.*, 2019, **783**, 193–207; doi:https://doi.org/10.1016/j.jallcom.2018.12.300.
22. Komarasamy, M. *et al.*, A novel method to enhance CSL fraction, tensile properties and work hardening in complex concentrated alloys – lattice distortion effect. *Mater. Sci. Eng. A*, 2018, **736**, 383–391.
23. Ranganathan, S., Alloyed pleasures: multimetallic cocktails. *Curr. Sci.*, 2003, **85**, 1404–1406.
24. Anand, G., Wynn, A. P., Handley, C. M. and Freeman, C. L., Phase stability and distortion in high-entropy oxides. *Acta Mater.*, 2018, **146**, 119–125; doi:https://doi.org/10.1016/j.actamat.2017.12.037.
25. Zhang, Y. *et al.*, Dense high-entropy boride ceramics with ultra-high hardness. *Scr. Mater.*, 2019, **164**, 135–139; doi:https://doi.org/10.1016/j.scriptamat.2019.01.021.
26. Ding, H. Y. and Yao, K. F., High entropy $Ti_{20}Zr_{20}Cu_{20}Ni_{20}Be_{20}$ bulk metallic glass. *J. Non-Cryst. Solids*, 2013, **364**, 9–12; doi:https://doi.org/10.1016/j.jnoncrysol.2013.01.022.
27. Takeuchi, A., Chen, N., Wada, T., Yokoyama, Y., Kato, H., Inoue, A. and Yeh, J. W., $Pd_{20}Pt_{20}Cu_{20}Ni_{20}P_{20}$ high-entropy alloy as a bulk metallic glass in the centimeter. *Intermetallics*, 2011, **19**, 1546–1554; doi:https://doi.org/10.1016/j.intermet.2011.05.030.
28. Rost, C. M. *et al.*, Entropy-stabilized oxides. *Nature Commun.*, 2015, **6**, 8485; doi:https://doi.org/10.1038/ncomms9485.
29. Mao, A., Xiang, H.-Z., Zhang, Z.-G., Kuramoto, K., Yu, H. and Ran, S., Solution combustion synthesis and magnetic property of rock-salt $(Co_{0.2}Cu_{0.2}Mg_{0.2}Ni_{0.2}Zn_{0.2})O$ high-entropy oxide nanocrystalline powder. *J. Magn. Magn. Mater.*, 2019, **484**, 245–252; doi:https://doi.org/10.1016/j.jmmm.2019.04.023.
30. Sarkar, A. *et al.*, High-entropy oxides: fundamental aspects and electrochemical properties. *Adv. Mater.*, 2019, **31**, 1806236; doi:10.1002/adma.201806236.
31. Sarkar, A. *et al.*, Nanocrystalline multicomponent entropy stabilised transition metal oxides. *J. Eur. Ceram. Soc.*, 2017, **37**, 747–754; doi:https://doi.org/10.1016/j.jeurceramsoc.2016.09.018.
32. Sarkar, A. *et al.*, High entropy oxides for reversible energy storage. *Nature Commun.*, 2018, **9**, 3400; doi:https://doi.org/10.1038/s41467-018-05774-5.
33. Sharma, Y. *et al.*, Single-crystal high entropy perovskite oxide epitaxial films. *Phys. Rev. Mater.*, 2018, **2**, 060404(R); doi:10.1103/PhysRevMaterials.2.060404.
34. Castle, E., Csanádi, T., Grasso, S., Dusza, J. and Reece, M., Processing and properties of high entropy ultra-high temperature carbides. *Sci. Rep.*, 2018, **8**, 8609; doi:10.1038/s41598-018-26827-1.
35. Gild, J. *et al.*, High-entropy metal diborides: a new class of high-entropy materials and a new type of ultrahigh temperature ceramics. *Sci. Rep.*, 2016, **6**, 37946; doi:10.1038/srep37946.
36. Martyushev, L. M., The maximum entropy production principle: two basic questions. *Philos. Trans. R. Soc. London, Ser. B*, 2010, **365**, 1333–1334; doi:https://doi.org/10.1098/rstb.2009.0295.
37. Wang, Z., Guo, S. and Liu, C. T., Phase selection in high-entropy alloys: from nonequilibrium to equilibrium. *J. Mater.*, 2014, **66**, 1966–1972; doi:https://doi.org/10.1007/s11837-014-0953-8.
38. Guo, S., Phase selection rules for cast high entropy alloys: an overview. *Mater. Sci. Technol.*, **31**(10), 1223–1230; doi:10.1179/1743284715Y.0000000018.
39. Zhang, Y., Zhou, Y. J., Lin, J. P., Chen, G. L. and Liaw, P. K., Solid-solution phase formation rules for multi-component alloys. *Adv. Eng. Mater.*, 2008; doi:https://doi.org/10.1002/adem.200700240.
40. Yang, X. and Zhang, Y., Prediction of high-entropy stabilized solid-solution in multi-component alloys. *Mater. Chem. Phys.*, 2012, **132**, 233–238; doi:10.1016/j.matchemphys.2011.11.021.
41. Mansoori, G. A., Carnahan, N. F., Starling, K. E. and Leland, T. W., Equilibrium thermodynamic properties of the mixture of hard

spheres. *J. Chem. Phys.*, 1971, **54**, 1523; doi:https://doi.org/10.1063/1.1675048.
42. Raghavan, R., Hari Kumar, K. C. and Murty, B. S., Analysis of phase formation in multi-component alloys. *J. Alloys Compd.*, 2012, **544**, 152–158; doi:https://doi.org/10.1016/j.jallcom.2012.07.105.
43. Raghavan, R., Hari Kumar, K. C. and Murty, B. S., Analysis of phase formation in multi-component alloys. *J. Alloys Compd.*, 2012, **544**, 152–158; doi:https://doi.org/10.1016/j.jallcom.2012.07.105.
44. Wang, Z., Huang, Y., Yang, Y., Wang, J. and Liu, C. T., Atomic-size effect and solid solubility of multicomponent alloys. *Scr. Mater.*, 2015, **94**, 28–31; doi:https://doi.org/10.1016/j.scriptamat.2014.09.010.
45. Allison, J., Backman, D. and Christodoulou, L., Integrated computational materials engineering: a new paradigm for the global materials profession. *J. Mater.*, 2006, **58**, 25–27; doi:https://doi.org/10.1007/s11837-006-0223-5.
46. https://www.nist.gov/mgi
47. Olson, G. B. and Kuehmann, C. J., Materials genomics: from CALPHAD to flight. *Scr. Mater.*, 2014, **70**, 25–30; doi:https://doi.org/10.1016/j.scriptamat.2013.08.032.
48. Jain, A., Persson, K. A. and Ceder, G., Research update: the materials genome initiative: data sharing and the impact of collaborative *ab initio* databases. *APL Mater.*, 2016, **4**, 053102; doi:https://doi.org/10.1063/1.4944683.
49. Kattner, U. R., The thermodynamic modeling of multicomponent phase equilibria. *J. Mater.*, 1997, **49**, 14–19; doi:https://doi.org/10.1007/s11837-997-0024-5.
50. Saunders, N. and Miodownik, A. P., *CALPHAD (Calculation of Phase Diagrams): A Comprehensive Guide*, Pergamon, UK, 1998.
51. Gao, M. C. and Alman, D. E., Searching for next single-phase high-entropy alloy compositions. *Entropy*, 2013, **15**, 4504–4519; doi: https://doi.org/10.3390/e15104504.
52. Tazuddin, Gurao, N. P. and Biswas, K., In the quest of single phase multi-component multiprincipal high entropy alloys. *J. Alloys Compd.*, 2017, **697**, 434–442; doi:https://doi.org/10.1016/j.jallcom.2016.11.383.
53. Sonkusare, R., Divya Janani, P., Gurao, N. P., Sarkar, S., Sen, S., Pradeep, K. G. and Biswas, K., Phase equilibria in equiatomic CoCuFeMnNi high entropy alloy. *Mater. Chem. Phys.*, 2018, **210**, 269–278; doi:https://doi.org/10.1016/j.matchemphys.2017.08.051.
54. Raturi, A., Aditya, J., Gurao, N. P. and Biswas, K., ICME approach to explore equiatomic and non-equiatomic single phase BCC refractory high entropy alloys. *J. Alloys Comps.*, 2019, **806**, 587–595; doi:https://doi.org/10.1016/j.jallcom.2019.06.387.
55. Li, Z., Körmann, F., Grabowski, B., Neugebauer, J. and Raabe, D., *Ab initio* assisted design of quinary dual-phase high-entropy alloys with transformation-induced plasticity. *Acta Mater.*, 2017, **136**, 262–270; doi:https://doi.org/10.1016/j.actamat.2017.07.023.
56. Ikeda, Y., Grabowski, B. and Körmann, F., *Ab initio* phase stabilities and mechanical properties of multicomponent alloys: a comprehensive review for high entropy alloys and compositionally complex alloys. *Mater. Charact.*, 2019, **147**, 464–511; doi:https://doi.org/10.1016/j.matchar.2018.06.019.
57. Otto, F., Dlouhy, A., Somsen, C., Bei, H., Eggeler, G. and George, E. P., The influence of temperature and microstructure on the tensile properties of a CoCrFeMnNi high-entropy alloy. *Acta Mater.*, 2013, **61**, 5743–5755; doi:https://doi.org/10.1016/j.actamat.2013.06.018.
58. Laplanche, G., Kostka, A., Horst, O. M., Eggeler, G. and George, E. P., Microstructure evolution and critical stress for twinning in the CrMnFeCoNi high-entropy alloy. *Acta Mater.*, 2016, **118**, 152–163; doi:https://doi.org/10.1016/j.actamat.2016.07.038.
59. Komarasamy, M., Kumar, N., Mishra, R. S. and Liaw, P. K., Anomalies in the deformation mechanism and kinetics of coarse-grained high entropy alloy. *Mater. Sci. Eng. A*, 2016, **654**, 256–263; https://doi.org/10.1016/j.msea.2015.12.063.
60. Gludovatz, B., Hohenwarter, A., Catoor, D., Chang, E. H., George, E. P. and Ritchie, R. O., A fracture-resistant high-entropy alloy for cryogenic applications. *Science*, 2014, **345**, 1153–1158; doi:10.1126/science.1254581.
61. Li, Z., Pradeep, K. G., Deng, Y., Raabe, D. and Tasan, C. C., Metastable high-entropy dual-phase alloys overcome the strength–ductility trade-off. *Nature*, 2016, **534**, 227–230; doi:10.1038/nature17981.
62. Raabe, D., Tasan, C. C., Springer, H. and Bausch, M., From High-entropy alloys to high-entropy steels. *Steel Res. Int.*, 2015, **86**, 1127–1138; doi:https://doi.org/10.1002/srin.201500133.
63. Agarwal, R., Sonkusare, R., Jha, S. R., Gurao, N. P., Biswas, K. and Nayan, N., Understanding the deformation behavior of CoCuFeMnNi high entropy alloy by investigating mechanical properties of binary ternary and quaternary alloy subsets. *Mater. Des.*, 2018, **157**, 539–550; doi:https://doi.org/10.1016/j.matdes.2018.07.046.
64. Sonkusare, R. *et al.*, Establishing processing–microstructure–property paradigm in complex concentrated equiatomic CoCuFeMnNi alloy. *Mater. Sci. Eng. A*, 2019, **759**, 415–429; doi:https://doi.org/10.1016/j.msea.2019.04.096.
65. Tazuddin, Biswas, K. and Gurao, N. P., Deciphering micro-mechanisms of plastic deformation in a novel single phase fcc-based MnFeCoNiCu high entropy alloy using crystallographic texture. *Mater. Sci. Eng. A*, 2016, **657**, 224–233; doi:https://doi.org/10.1016/j.msea.2016.01.065.
66. Sonkusare, R., Khandelwal, N., Biswas, K. and Gurao, N. P., A comparative study on the evolution of microstructure and hardness during monotonic and cyclic high pressure torsion of CoCuFeMnNi high entropy alloy. *J. Mater. Res.*, 2019, **34**, 732–743; doi:https://doi.org/10.1557/jmr.2018.479.
67. Senkov, O. N. and Semiatin, S. L., Microstructure and properties of a refractory high-entropy alloy after cold working. *J. Alloys Compd.*, 2015, **649**, 1110–1123; doi:https://doi.org/10.1016/j.jallcom.2015.07.209.
68. Senkov, O. N., Wilks, G. B., Scott, J. M. and Miracle, D. B., Mechanical properties of $Nb_{25}Mo_{25}Ta_{25}W_{25}$ and $V_{20}Nb_{20}Mo_{20}Ta_{20}W_{20}$ refractory high entropy alloys. *Intermetallics*, 2011, **19**, 698–706; doi:https://doi.org/10.1016/j.intermet.2011.01.004.
69. Mohanty, S., Gurao, N. P. and Biswas, K., Sinter ageing of equiatomic $Al_{20}Co_{20}Cu_{20}Zn_{20}Ni_{20}$ high entropy alloy via mechanical alloying. *Mater. Sci. Eng. A*, 2014, **617**, 211–218; doi:https://doi.org/10.1016/j.msea.2014.08.046.
70. Mohanty, S., Gurao, N. P., Padaikathan, P. and Biswas, K., Ageing behaviour of equiatomic consolidated $Al_{20}Co_{20}Cu_{20}Ni_{20}Zn_{20}$ high entropy alloy. *Mater. Character.*, 2017, **129**, 127–134; doi:https://doi.org/10.1016/j.matchar.2017.04.011.
71. Mohanty, S., Maity, T. N., Mukhopadhyay, S., Sarkar, S., Gurao, N. P., Bhowmick, S. and Biswas, K., Powder metallurgical processing of equiatomic AlCoCrFeNi high entropy alloy: microstructure and mechanical properties. *Mater. Sci. Eng. A*, 2017, **679**, 299–313; doi:https://doi.org/10.1016/j.msea.2016.09.062.
72. Yadav, S., Aggrawal, A., Kumar, A. and Biswas, K., Effect of TiB_2 addition on wear behavior of $(AlCrFeMnV)_{90}Bi_{10}$ high entropy alloy composite. *Tribol. Int.*, 2019, **132**, 62–74; doi:https://doi.org/10.1016/j.triboint.2018.11.025.
73. Yadav, S., Sarkar, S., Aggarwal, A., Kumar, A. and Biswas, K., Wear and mechanical properties of novel $(CuCrFeTiZn)_{100-x}Pb_x$ high entropy alloy composite via mechanical alloying and spark plasma sintering. *Wear*, 2018, **410–411**, 93–109; doi:https://doi.org/10.1016/j.wear.2018.05.023.
74. Yadav, S., Kumar, A. and Biswas, K., Wear behavior of high entropy alloys containing soft dispersoids (Pb, Bi). *Mater. Chem. Phys.*, 2018, **210**, 222–232; doi:https://doi.org/10.1016/j.matchemphys.2017.06.020.

75. Hemphill, M. A., Yuan, T., Wang, G. Y., Yeh, J. W., Tsai, C. W., Chuang, A. and Liaw, P. K., Fatigue behavior of $Al_{0.5}$CoCrCuFeNi high entropy alloys. *Acta Mater.*, 2012, **60**, 5723–5734; doi:https://doi.org/10.1016/j.actamat.2012.06.046.
76. Tang, Z., Yuan, T., Tsai, C.-W., Yeh, J.-W., Lundin, C. D. and Liaw, P. K., Fatigue behavior of a wrought $Al_{0.5}$CoCrCuFeNi two-phase high-entropy alloy. *Acta Mater.*, 2015, **99**, 247–258; doi:https://doi.org/10.1016/j.actamat.2015.07.004.
77. Bahadur, F., Biswas, K. and Gurao, N. P., Micro-mechanisms of microstructural damage due to low cycle fatigue in CoCuFeMnNi high entropy alloy. *Int. J. Fatigue*, 2020, **130**, 105258; doi:https://doi.org/10.1016/j.ijfatigue.2019.105258.
78. Schuh, B., Mendez-Martin, F., Völker, B., George, E. P., Clemens, H., Pippan, R. and Hohenwarter, A., Mechanical properties, microstructure and thermal stability of a nanocrystalline CoCrFeMnNi high-entropy alloy after severe plastic deformation. *Acta Mater.*, 2015, **96**, 258–268; doi:https://doi.org/10.1016/j.actamat.2015.06.025.
79. Zhang, Y., Zuo, T, Cheng, Y. and Liaw, P. K., High-entropy Alloys with high saturation magnetization, electrical resistivity and malleability. *Sci. Rep.*, 2013, **3**, 1455; doi:10.1038/srep01455.
80. Yuan, Y. *et al.*, Rare-earth high-entropy alloys with giant magnetocaloric effect. *Acta Mater.*, 2017, **125**, 481–489; doi:https://doi.org/10.1016/j.actamat.2016.12.021.
81. Mazur, Y. P., Ostapenko, R. V. and Semenko, M. P., Influence of a cold plastic deformation on the electrical resistivity of CrMnFeCoNi high entropy alloy. *Ukr. J. Phys.*, 2017, **62**, 413–421; doi:https://doi.org/10.15407/ujpe62.05.0413.
82. Gao, M. C., Miracle, D. B., Maurice, D. and Yan, X., High-entropy functional materials. *J. Mater. Res.*, 2018, **33**, 3138–3155; doi:https://doi.org/10.1557/jmr.2018.323.
83. Shafeie, S., Guo, S., Hu, Q., Fahlquist, H., Erhart, P. and Palmqvist, A., High-entropy alloys as high-temperature thermoelectric materials. *J. Appl. Phys.*, 2015, **118**, 184905; doi:https://doi.org/10.1063/1.4935489.
84. Karlsson, D. *et al.*, Structure and hydrogenation properties of a HfNbTiVZr high entropy alloy. *Inor. Chem.*, 2018, **57**, 2103–2113; doi:https://doi.org/10.1021/acs.inorgchem.7b03004.
85. Zhang, G., Ming, K., Kang, J., Huang, Q., Zhang, Z., Zheng, X. and Bi, X., High entropy alloy as a highly active and stable electrocatalyst for hydrogen evolution reaction. *Electrochim. Acta*, 2018, **279**, 19–23; doi:https://doi.org/10.1016/j.electacta.2018.05.035.
86. Wang, Z. and Baker, I., Interstitial strengthening of a FCC FeNiMnAlCr high entropy alloy. *Mater. Lett.*, 2016, **180**, 153–156; doi:https://doi.org/10.1016/j.matlet.2016.05.122.
87. Li, Z., Tasan, C. C., Springer, H., Gault, B. and Raabe, D., Interstitial atoms enable joint twinning and transformation induced plasticity in strong and ductile high-entropy alloys. *Sci. Rep.*, 2017, **7**, 40704; doi:10.1038/srep40704.
88. Li, Z., Zhao, S., Ritchie, R. O. and Meyers, M. A., Mechanical properties of high-entropy alloys with emphasis on face-centered cubic alloys. *Prog. Mater. Sci.*, 2019, **102**, 296–345; doi:https://doi.org/10.1016/j.pmatsci.2018.12.003.
89. Zhang, Y., Zuo, T. T., Tang, Z., Gao, M. C., Dahmen, K. A., Liaw, P. K. and Lu, Z. P., Microstructures and properties of high-entropy alloys. *Prog. Mater. Sci.*, 2014, **61**, 1–93; doi:https://doi.org/10.1016/j.pmatsci.2013.10.001.
90. Zhang, R.-Z. and Reece, M. J., Review of high entropy ceramics: design, synthesis, structure and properties. *J. Mater. Chem. A*, 2017, **7**, 22148–22162; doi:10.1039/C9TA05698J.
91. McDowell, D. L. and Olson, G. B., Concurrent design of hierarchical materials and structures. *Sci. Model. Simul.*, 2010, 207–240; doi:10.1007/978-1-4020- 9741-6_14.
92. Gorsse, S. and Tancret, F., Current and emerging practices of CALPHAD toward the development of high entropy alloys and complex concentrated alloys. *J. Mater. Res.*, 2018, **33**, 2899–2923; doi:https://doi.org/10.1557/jmr.2018.152.
93. Tian, F., A review of solid-solution models of high-entropy alloys based on *ab initio* calculations. *Fronti. Mater.*, 2017, **4**, 36; doi:https://doi.org/10.3389/fmats.2017.00036.
94. http://www.dierk-raabe.com/steels-brief-introduction/
95. Guo, S. and Liu, C. T., Phase stability in high entropy alloys: formation of solid solution phase or amorphous phase. *Prog. Nat. Sci.*, 2011, **21**, 433–446; doi:https://doi.org/10.1016/S1002-0071(12)60080-X.
96. Guo, S., Hu, Q., Ng, C. and Liu, C. T., More than entropy in high-entropy alloys: forming solid solutions or amorphous phase. *Intermetallics*, 2013, **41**, 96–103; doi:https://doi.org/10.1016/j.intermet.2013.05.002.
97. Ren, M. X., Li, B. S. and Fu, H. Z., Formation condition of solid solution type high-entropy alloy. *Trans. Nonferrous Met. Soc. China*, 2013, **23**, 991–995; doi:10.1016/S1003-6326(13)62557-1.

ACKNOWLEDGEMENTS. We thank our research students, funding agencies (DST-SERB, ISRO, BRNS) and colleagues for discussions and constructive criticisms. We thank Ms Reshma Sonkusare (IIT, Kanpur) for proof reading the manuscript and Prof. Satyam Suwas (IISc, Bengaluru) for completion of the review in time. We also thank Profs Rangnathan, B. S. Murty, N. K. Mukhopadhyay, B. Basu, R. S. Mishra, J. W. Yeh for constant encouragement and support.

Received 2 December 2019; accepted 1 January 2020

doi: 10.18520/cs/v118/i10/1520-1539